A Volcano Rekindled: The Renewed Eruption of Mount St. Helens, 2004–2006
Edited by David R. Sherrod, William E. Scott, and Peter H. Stauffer
U.S. Geological Survey Professional Paper 1750, 2008

Chapter 22

Constraints on the Size, Overpressure, and Volatile Content of the Mount St. Helens Magma System from Geodetic and Dome-Growth Measurements During the 2004–2006+ Eruption

By Larry G. Mastin[1], Evelyn Roeloffs[1], Nick M. Beeler[1], and James E. Quick[2]

Abstract

During the ongoing eruption at Mount St. Helens, Washington, lava has extruded continuously at a rate that decreased from ~7–9 m^3/s in October 2004 to 1–2 m^3/s by December 2005. The volume loss in the magma reservoir estimated from the geodetic data, $1.6–2.7\times10^7$ m^3, is only a few tens of percent of the 7.5×10^7 m^3 volume that had erupted by the end of 2005.

In this paper we use geodetic models to constrain the size and depth of the magma reservoir. We also ask whether the relations between extruded volume and geodetic deflation volume are consistent with drainage of a reservoir of compressible magma within a linearly elastic host rock. Finally, we compare the time histories of extrusion and geodetic deflation with idealized models of such a reservoir. Critical parameters include erupted volume V_e, dome density ρ_e, reservoir volume V_C, initial reservoir overpressure p_0^{ex}, pressure drop during the eruption Δp, reservoir compressibility $\kappa_C \equiv (1/V_C)(dV_C / dp)$, magma density ρ_M, and magma compressibility $\kappa_M \equiv (1/\rho_M)(d\rho_M/dp)$. Seismic velocity and reservoir geometry suggest $\kappa_C \approx 2\times10^{-11}$ Pa^{-1}, but mechanical considerations suggest $\kappa_C = 7–15\times10^{-11}$ Pa^{-1}.

The geodetic data are best fit with an ellipsoidal source whose top is 5±1 km deep and whose base is ~10–20+ km deep. In the absence of recharge, the decrease in magma-reservoir volume dV_C is theoretically related to the erupted volume V_e by $V_e/dV_C = (\rho_M/\rho_e)(1+\kappa_M/\kappa_C)$. For $\kappa_C = \sim7–15\times10^{-11}$ Pa^{-1} and $\rho_M \approx \rho_e$, estimates of V_e and dV_C suggest that $\kappa_M = 1.4–3.0\times10^{-10}$ Pa^{-1}, corresponding to a magmatic gas content in the reservoir of $v_g = 0$ to 1.8 percent by volume.

If we assume that effusion rate is linearly related to reservoir pressure and that the recharge rate into the reservoir is constant, the effusion rate should decrease exponentially with time to a value that equals the recharge rate. Best-fit curves of this form suggest recharge rates of 1.2–1.3 m^3/s over the first 500 days of the eruption. The best-fit constants include the product $V_C p_0^{ex} (\kappa_C + \kappa_M)$, making it possible to constrain reservoir volume using values of κ_C and κ_M constrained from ratios of erupted volume to geodetic deflation volume. If, on the other hand, we assume a logarithmic pressure-effusion rate relation and a constant recharge rate, the dome volume-time curve should follow a modified logarithmic relation, with the total erupted volume at a given time proportional to $V_C \Delta p (\kappa_C + \kappa_M)$. Using $\kappa_C = 7–15\times10^{-11}$ Pa^{-1}, results from log and exponential curves suggest a reservoir volume of at least several cubic kilometers if Δp or p_0^{ex} is less than ~30 MPa. Similar results are obtained from numerical calculations that consider temporal changes in (1) magma compressibility, (2) the weight of the lava dome suppressing effusion, and (3) recharge rate. These results are consistent with the notion that the reservoir volume is at least a few times larger than the largest Holocene eruption of Mount St. Helens (4 km^3 dense-rock-equivalent + volume for the 3.4-ka Yn eruption).

Both the exponential and logarithmic models predict a history of reservoir decompression that imperfectly matches displacement data at GPS station JRO1. Neither model, for example, predicts the rapid radially inward movement at JRO1 during the first month of the eruption. Such movement, followed by long-term linear deflation, suggests that erupted magma has been replaced in increasing proportions by recharge, but that the recharge rate remains somewhat less than the current (early 2006) effusion rate.

[1] U.S. Geological Survey, 1300 SE Cardinal Court, Vancouver, WA 98683

[2] U.S. Geological Survey, Reston, VA 20192; now at Southern Methodist University, Office of Research and Graduate Studies, P.O. Box 750240, Dallas, Texas 75275

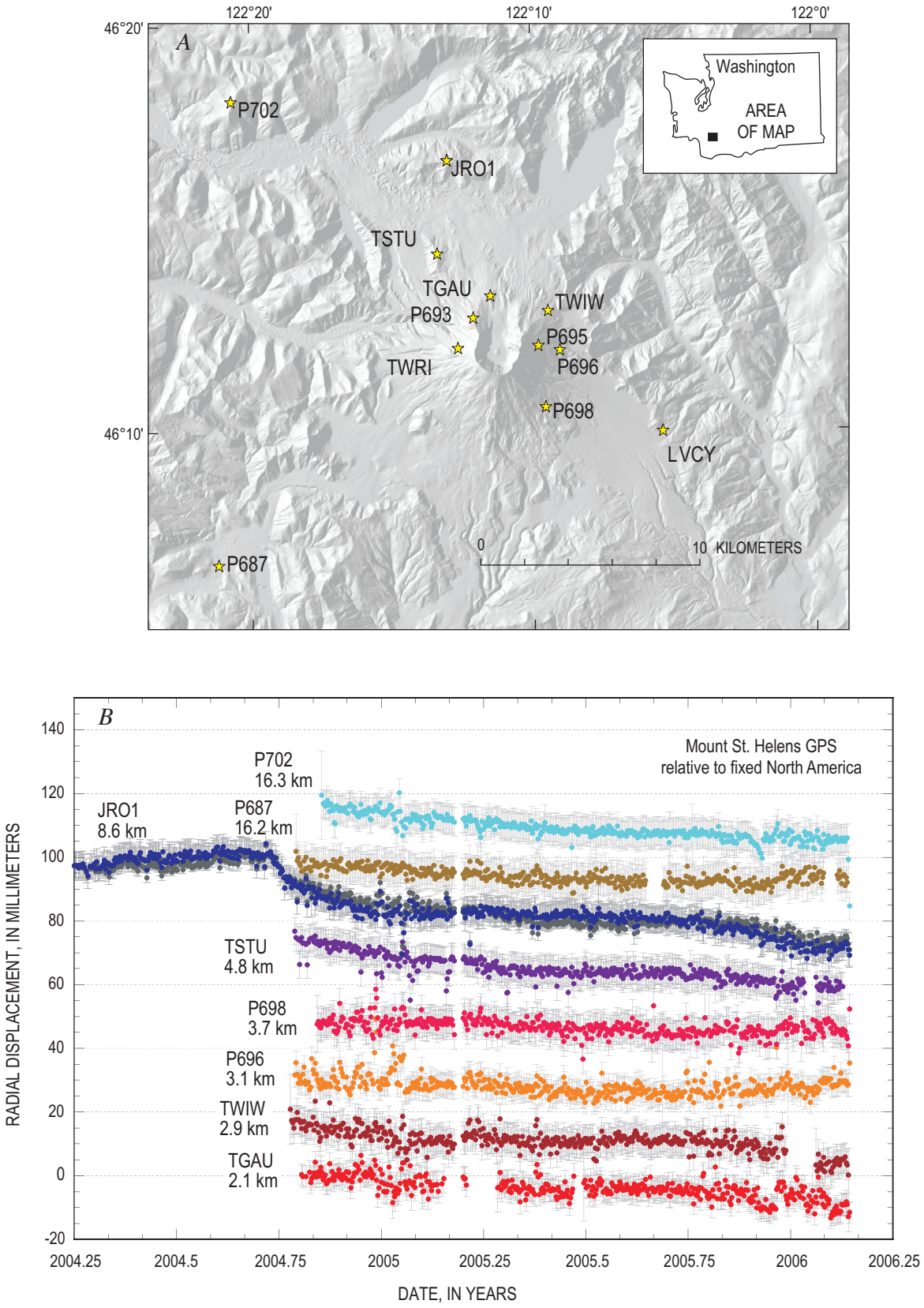

Figure 1. Geodetic stations and results. *A*, Map showing geodetic stations used to model the source of deflation at Mount St. Helens. *B*, Displacement radial to the Mount St. Helens crater versus time at geodetic stations. Outward radial displacements are positive. Error bars represent one standard deviation above and below the data point. Numbers beneath each station label indicate the map distance of each station from the crater center (46.2002° N, 122.1911° W).

Introduction

The current Mount St. Helens eruption extruded about 85 percent as much lava in 14 months (October 2004 to December 2005) as was extruded in 6 years to form the 1980–86 lava dome. At the time of writing (spring 2006), there is no obvious indication of waning growth; indeed, compared with other dome-building eruptions worldwide, the current eruption of Mount St. Helens only slightly exceeds the median duration (540 days) and volume (3.5×10^7 m^3) among historical dome-building eruptions (Newhall and Melson, 1983, and updates, C. Newhall, written commun., 2005). This eruption hardly approaches the duration (>50 years) of the dome building at Bezymianny Volcano, Kamchatka, whose growth followed a sector collapse and lateral blast in 1956 that resembled the 1980 Mount St. Helens sequence.

Dome-building eruptions, like eruptions of mafic lava flows, range in duration from days to decades and in volume from cubic meters to cubic kilometers. Eruption volume and duration are most strongly controlled by reservoir size, exsolved gas content, the amount of recharge into the magma system, and the composition and volatile content of recharging magma (Wadge, 1981; Newhall and Melson, 1983; Huppert and Woods, 2002; Woods and Huppert, 2003). In this study we use geodetic and growth-history data to constrain the volume, overpressure, history of recharge, and exsolved volatile content of the Mount St. Helens magma system.

Key Observations

Over several years prior to September 2004, campaign-style geodetic surveys and measurements at the only continuous global positioning system (CGPS) site at Mount St. Helens (JRO1, fig. 1*A*) showed no discernable inflation signal (Dzurisin and others, this volume, chap. 14; Lisowski and others, this volume, chap. 15). Deflation at JRO1 began with the onset of seismicity on September 23, 2004; uplift on the crater floor was first noticed on about September 26 (Dzurisin and others, this volume, chap. 14) and the first material at magmatic temperature on October 11. Eight new CGPS instruments installed between mid-October and early November 2004 (fig. 1*A*) have recorded more or less radially inward movement toward the crater (fig. 1), suggesting that the source of deflation (the magma reservoir) is roughly spherical or elliptical in shape rather than dike-shaped (Lisowski and others, this volume, chap. 15).

Throughout the eruption, lava has extruded as spines or lobes of more or less solid, nearly holocrystalline lava, their surfaces covered by unconsolidated fault gouge on the order of 1 m thick (fig. 2). The gouge thickness, considering relations between gouge thickness and displacement on tectonic faults (Robertson, 1983; Power and others, 1988), and petrologic information (Cashman and others, this volume, chap. 19) suggest that the faulting may extend from perhaps tens of meters to several hundred meters into the subsurface.

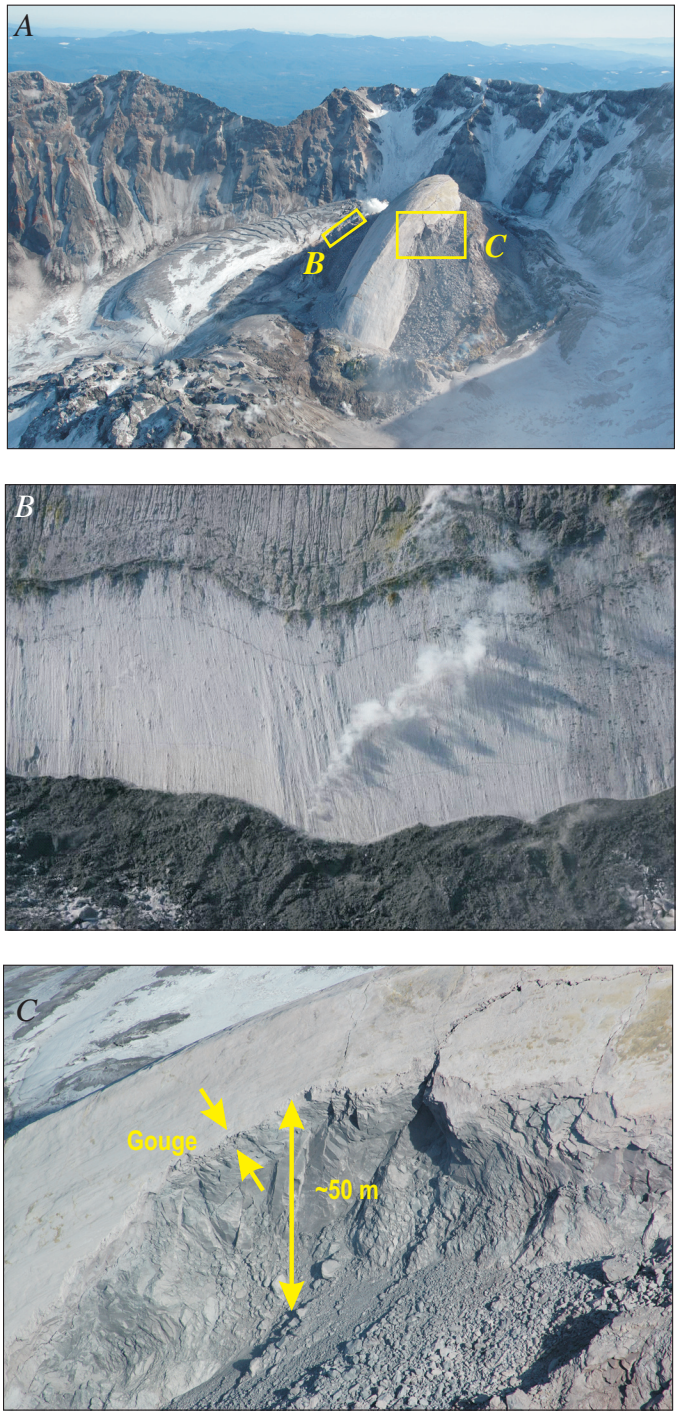

Figure 2. Photos of the growing lava dome of Mount St. Helens. *A*, View of spine 4 from the northwest on February 22, 2005. USGS photo by S.P. Schilling. *B*, Close-up of striated fault gouge covering the exterior of spine 3 as it emerged from the ground on November 11, 2004. Approximate location of that spine on February 22, 2005, shown by box *B* on panel *A*. USGS photo by J.S. Pallister. *C*, Close-up of fresh rockfall scar (~100 m long and 50 m high), revealing gouge thickness in cross section. Approximate location shown by box *C* on panel *A*. USGS photo taken February 22, 2005, by S.P. Schilling.

A series of digital elevation models (DEMs) based on 1:12,000-scale aerial photographs records the growth of the lava dome (Schilling and others, this volume, chap. 8). These DEMs show that in early October 2004 the rate of uplift of cold rock and glacial ice was on the order of 8–9 m^3/s, with nearly 1.1×10^7 m^3 uplifted by the time lava first became visible at the surface on October 11. Lava ("hot rock") extrusion rates were initially ~6–7 m^3/s in November 2004 but declined to less than 2 m^3/s in March 2005. Since March 2005 (about 150 days into the eruption) the extrusion rate has continued to decline gradually, such that the volume-time curve can be nearly fit with a straight line (fig. 3). Overall, the history of lava-dome volume versus time (fig. 3) has defined a remarkably regular monotonic, concave-downward curve that was noted in early 2005 and could be fit using simple exponential (fig. 3*C*) and logarithmic (fig. 3*A*) curves. In this study we endeavor to find the physical basis for these curve forms.

Geodetic Source Models

Using data from eight continuous GPS stations (fig. 1), we estimate the depth, location, and size of the source of deflation (the magma reservoir) by comparing inward displacements with those predicted for a vertical prolate ellipsoid embedded in a homogeneous, isotropic, linearly elastic half-space, using the equations of Bonaccorso and Davis (1999) (table 1). We evaluate the displacements during two time windows: (1) November 4, 2004, to February 5, 2005, and (2) February 5, 2005, to July 14, 2005. The start and end dates of these windows were chosen to coincide with DEM acquisition dates. We use only two time windows because data quality is insufficient to allow subdivision into shorter time windows. The second time window ends in summer 2005 because displacements since that time have been too small to be accurately modeled.

Measured displacements were adjusted for regional plate movement using the rates 3.461 mm/yr east, 5.91 mm/yr north, 1.46 mm/yr down; and for seasonal changes using sinusoidal adjustments having east, north, and z (vertical) amplitudes of 1.9149, 1.667, and 1.5289 mm and phase angles relative to January 1, 2004, of 51.86, 132.89, and 32.62 degrees, respectively (Lisowski and others, this volume, chap. 15). For the first time window, best-fit models place the top of the reservoir at 3–6 km below the mean altitude of the geodetic stations (which is ~1,300 m above sea level). In plan view the best-fit models lie 1.3–1.6 km east and 5–320 m south of the crater center (figs. 4, 5; table 1). Placing the top deeper than about 6 km tends to underestimate the radial displacement at stations proximal to the crater and overestimate both radial and vertical displacement components in the distal stations. The depth to the bottom of the reservoir is not well constrained but likely lies somewhere below 10 km (fig. 4*A*). Data from the second time period provide significantly poorer constraints (fig. 4*B*).

Geodetic Constraints on Reservoir Size and Pressure Drop

The amplitude of the geodetic signal scales with the product $R^2\Delta p/G$, where R is the horizontal radius of the ellipsoid, Δp is the pressure drop, and G is the host-rock shear modulus. Best-fit values of this product are listed in table 1. Using formulas for ellipsoid volume $V_C=(2/3)\pi R^2 h$ (where h is ellipsoid height) and elastic volume change of the ellipsoid $\Delta V_C=3V_C\Delta p/(4G)$ (McTigue, 1987; Tait and others, 1989; Tiampo and others, 2000), we find that $\Delta V_C=(\pi h/2)[R^2\Delta p/G]$. For the first time window, excluding sources at 4–7 km and 10–14 km depth that clearly do not fit the data, estimates of volume shrinkage of the magma body are $2.1–3.5\times10^6$ m^3. By comparison, the hot-rock volume (ΔV_e) erupted during this time (Schilling and others, this volume, chap. 8; and fig. 3) was about 2.7×10^7 m^3—eight to twelve times the volume shrinkage of the reservoir. For the second time window, $\Delta V_C=$ ~$3–8\times10^6$ m^3 (poorly constrained), whereas the change in dome volume was $\Delta V_e=1.8\times10^7$ m^3. For the entire eruption through late 2005, Lisowski and others (this volume, chap. 15) and Poland and Lu (this volume, chap. 18) estimate ΔV_C ~$1.6–2.7\times10^7$ m^3 from geodetic and InSAR data, whereas hot-rock erupted volume by mid-December 2005 was about 7.3×10^7 m^3 (Schilling and others, this volume, chap. 8). Differences in density of the erupted versus unerupted magma (estimated later) are not great enough to account for these discrepancies.

The reservoir volume and pressure drop can be constrained if the shear modulus G can be estimated. On the basis of estimated seismic P-wave velocity $v_P=6.7\pm0.2$ km/s at 8–15 km depth (Musumeci and others, 2002, fig. 5), host-rock density $\rho_R=2{,}700\pm200$ kg/m^3 (Williams and others, 1987), an assumed Poisson's ratio ν of 0.25 ± 0.03, and the formula $G=\rho_R v_P^2(1–2\nu)/(2(1–\nu))$ (for example, Rubin, 1990), we obtain $G=40\pm4$ GPa. Using this value and $\Delta V_C=2.3\times10^7$ m^3 in the formula $\Delta V_C=3V_C\Delta p/(4G)$, we obtain $V_C\Delta p=1.2\times10^{18}$ Pa·m^3. If we further assume that the pressure drop since the start of the eruption is less than a few tens of megapascals, the reservoir volume would have to exceed about 41 km^3—significantly larger than previously hypothesized at Mount St. Helens (>10 km^3 by Scandone and Malone, 1985; 5–7 km^3 by Barker and Malone, 1991). Several factors considered later and in appendix 1 suggest that a lower value of G, and hence smaller reservoir volume, is more appropriate.

An Idealized Magma Reservoir

We idealize the magma system (fig. 5) as an ellipsoidal magma body several kilometers deep within linearly elastic host rock, connected to the surface and to a source of recharge through relatively narrow conduits. The reservoir contains magma of density ρ_M and has a total mass $\rho_M V_C$. As long as the assumption of linear elastic host rock holds and the geometry of the reservoir does not change, the relation between

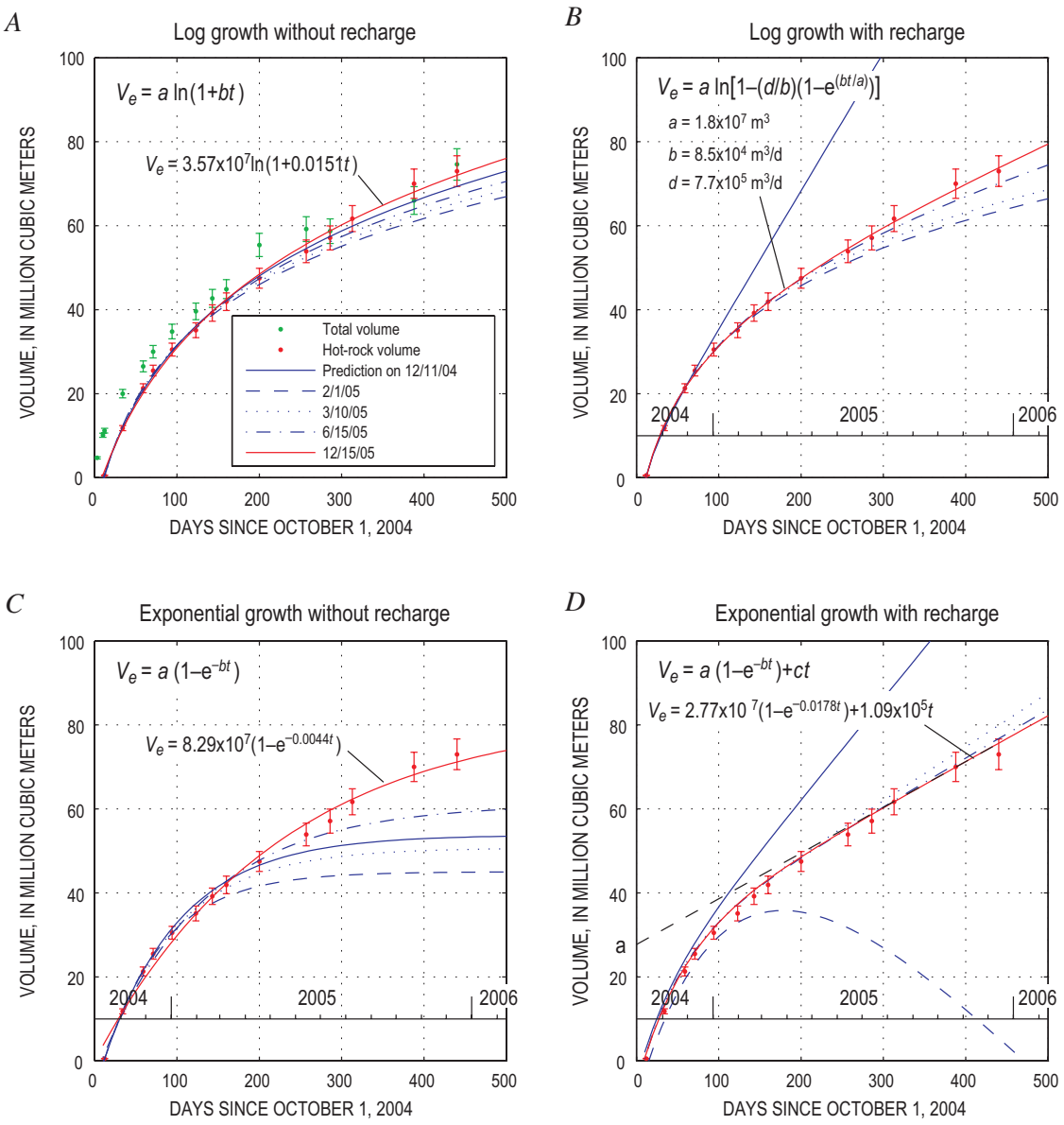

Figure 3. Lava dome volume (red dots) and total surface-deformation volume (green dots) versus time in days since October 1, 2004. Error bars are ±5 percent of the volume. Lines in each plot are fitted to a subset of data as of a certain date and then extrapolated onward as predictions. (Line of 12/11/04 is mostly extrapolation whereas line of 12/15/05 is mostly fitted.) Solid blue line fits volume measurements until about December 11, 2004; dashed blue line, February 1, 2005; dotted blue line, March 10, 2005; dot-dash blue line, June 15, 2005; solid red line, December 15, 2005. Plots *A*, *B*, *C*, and *D* show these best-fit curves using equations of different forms, shown in upper left corner of each plot. Terms *a*, *b*, *c*, and *d* in these equations are fitting coefficients; V_e is total erupted volume, and *t* is time since October 1, 2004.

Table 1. Parameters in geodetic source models plotted in figure 4.

[Parameters in plain type are specified by the user; those italicized are obtained by optimizing the fit between the model and the data.]

Model	Time period	Depth to top (m)	Depth to bottom (m)	Distance east of crater center (m)	Distance north of crater center (m)	Scale factor $\Delta pR^2/G$	$V_c\Delta p$ Pa•m^3 ×10^{17}	ΔV_c 10^6 m^3
1	11/4/04–2/5/05	*3,419*	20,000	*1,541*	*-68*	*-135*	-2.18	2.83
2	11/4/04–2/5/05	*3,654*	15,000	*1,511*	*-85*	*-155*	-1.72	3.69
3	11/4/04–2/5/05	*4,294*	10,000	*1,448*	*-100*	*-236*	-1.32	4.68
4	11/4/04–2/5/05	4,000	7,000	*1,492*	*-5*	*-286*	-0.84	1.80
5	11/4/04–2/5/05	6,000	10,000	*1,390*	*-321*	*-459*	-1.79	3.85
6	11/4/04–2/5/05	10,000	14,500	1,600	-500	*-885*	-3.89	8.34
7	2/5/05–7/14/05	3,500	15,500	1,400	-100	*-113*	-1.32	2.83
8	2/5/05–7/14/05	*7,191*	20,000	100	-3000	*-286*	-3.58	7.67

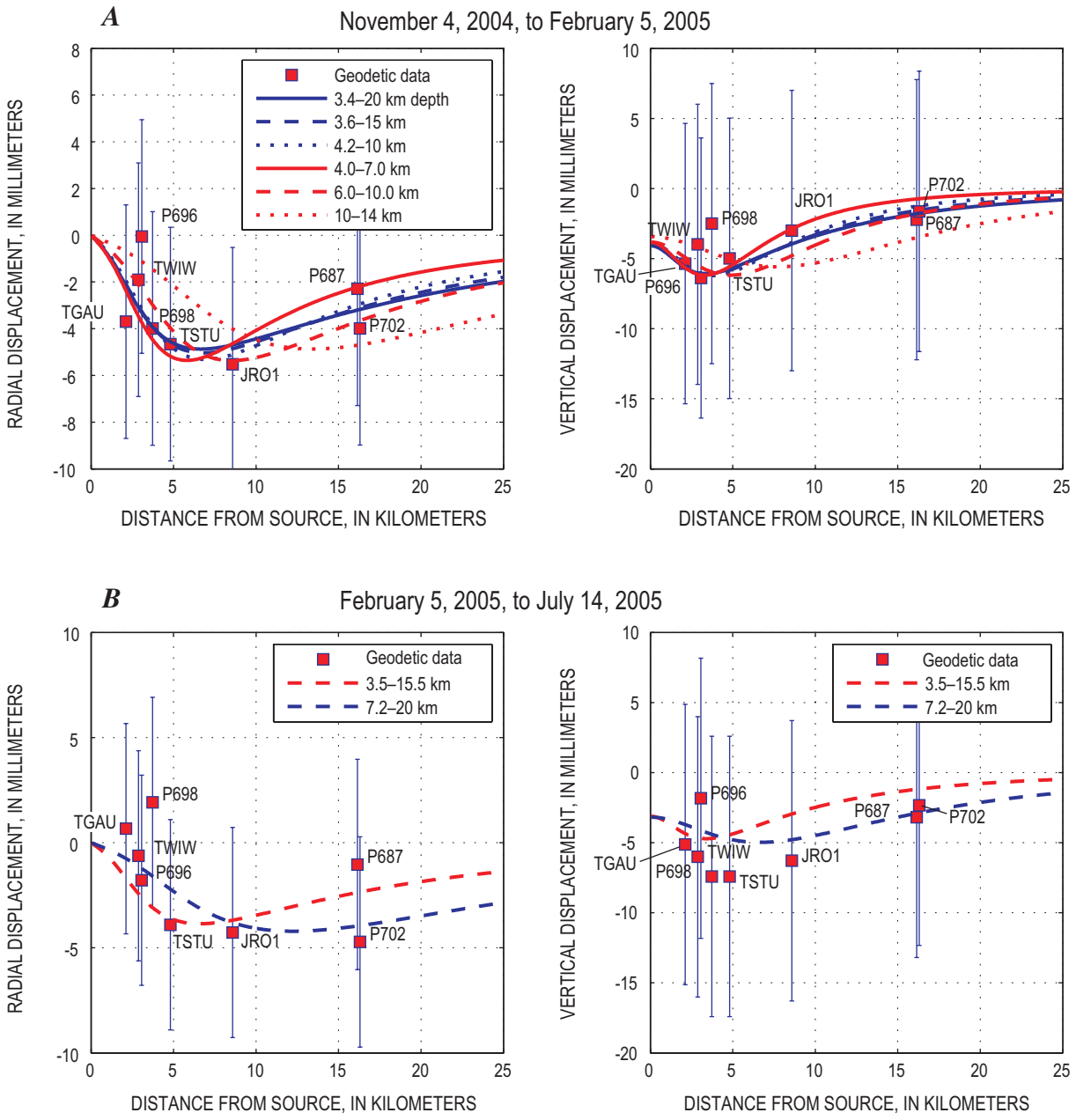

Figure 4 Measured and theoretical geodetic displacements for 252 days of eruption from November 4, 2004, to July 14, 2005. Data points, from continuous global positioning system (CGPS) receivers (fig 1*A*), show radial and vertical displacement; error bars are given as ±5 mm for radial displacement, ±10 mm for vertical displacement. Displacements are positive for outward radial and upward vertical directions. Lines represent theoretical displacements resulting from deflation of a vertical prolate ellipsoid in an elastic half-space. Depths in the explanation indicate, respectively, the depth to top and bottom of the ellipsoid below the mean altitude of the geodetic stations (1,300 m above sea level). *A*, Radial and vertical displacement between November 4, 2004, and February 5, 2005. *B*, Radial and vertical displacement between February 5 and July 14, 2005.

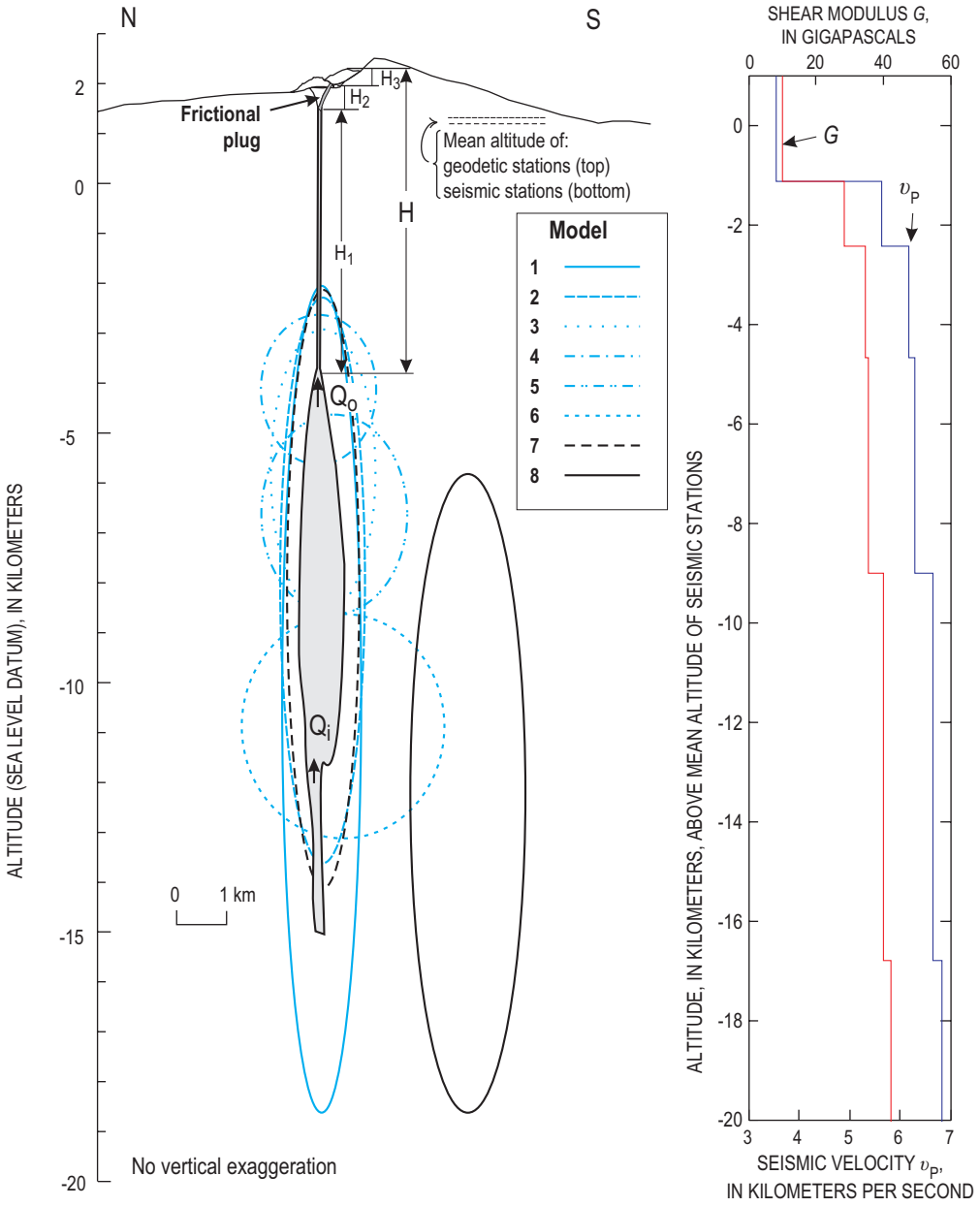

Figure 5. Left, Idealized north-south cross section through Mount St. Helens showing approximate location of the magma body (shaded), as judged from the geodetic modeling and some of the parameters used in this analysis. Blue and black dashed ellipses represent locations of geodetic models 1 through 8 listed in table 1; width of each ellipse represents its radius taken from value of $R^2\Delta p/G$ in table 1, using $\Delta p = 10$ MPa and $G = 35$ GPa. Right, Profile of seismic velocity (from Musumeci and others, 2002) and shear modulus G (estimated from seismic data and from density data of Williams and others, 1987). Shear modulus was estimated from the formula $G = \rho R v_p^2(1-2\nu)/(2(1-\nu))$, where Poisson's ratio, ν, is taken as 0.25 and ρ is taken as 2,150 kg/m^3 above the seismic datum and 2,700 kg/m^3 below it (Williams and others, 1987, fig. 8). Cross section and seismic profile have same vertical scales, but latter is set to datum of mean altitude of seismic stations.

reservoir pressure p and volume V_C is linear with a proportionality given by the reservoir compressibility κ_C:

$$\kappa_C \equiv \frac{1}{V_C}\frac{\partial V_C}{\partial p} \quad (1)$$

For a sphere or prolate ellipsoid, $\kappa_C = 3/(4G)$ (McTigue, 1987; Tiampo and others, 2000). We also assume that the magma has a finite compressibility (κ_M) given by:

$$\kappa_M \equiv \frac{1}{\rho_M}\frac{\partial \rho_M}{\partial p} . \quad (2)$$

Finally, we assume that the change in reservoir mass (dM_C) equals the mass added by recharge ($dM_i = \rho_i dV_i$) minus the mass erupted ($dM_e \approx \rho_e dV_e$), where ρ_i, ρ_e, dV_i, and dV_e are the densities and volumes of injected and erupted magma, respectively. In mathematical terms,

$$\begin{aligned} d\left(\rho_M V_C\right) &= \rho_M dV_C + V_C d\,\rho_M \\ &= -\rho_e dV_e + \rho_i dV_i \end{aligned} . \quad (3)$$

Adding terms for κ_C and κ_M into equation 3 and rearranging leads to:

$$dV_C = \frac{\rho_i dV_i - \rho_e dV_e}{\rho_M\left(1+\frac{\kappa_M}{\kappa_C}\right)} . \quad (4)$$

In the absence of recharge we have:

$$\frac{dV_e}{dV_C} = -\frac{\rho_M}{\rho_e}\left(1+\frac{\kappa_M}{\kappa_C}\right) . \quad (5)$$

Equation 5 carries the important implication that the erupted volume should not equal the volume shrinkage in the magma body except in the limiting case where the densities of erupted and unerupted magma are equal and the magma is incompressible ($\kappa_M \rightarrow 0$) (this was also pointed out by Johnson and others, 2000). If compressibility and density do not vary greatly with time during an eruption, equation 5 can be used to give the ratio of erupted volume V_e to the volume change of the magma reservoir ΔV_C. In spherical or ellipsoidal reservoirs, magma compressibility is generally thought to greatly exceed the reservoir compressibility (for example, Huppert and Woods, 2002); hence erupted volume should greatly exceed ΔV_C.

In the absence of recharge, what value of dV_e / dV_C might one expect at Mount St. Helens? The answer requires careful estimation of ρ_M, ρ_e, κ_M, and ρ_C, which we provide in the following several paragraphs.

The density of unerupted, volatile-saturated rhyolitic melt at ~200–250 MPa pressure is about 2,200 kg/m^3 (estimated using the method of Ghiorso and Sack in the program Conflow of Mastin, 2002). Combined with roughly 45 volume percent plagioclase crystals (Pallister and others, this volume, chap. 30) having a density of 2,600 kg/m^3, the bulk density of the magma ρ_M would be about 2,380 kg/m^3. Density measurements of most dome rock samples are about 2,300–2,500 kg/m^3 (K. Russell, written commun., 2006), although pores and voids could reduce the bulk density of the dome, ρ_e, by perhaps 10–20 percent below that of the dome rock. Within the uncertainties, we estimate the ratio ρ_M / ρ_e to be about 1.0 to 1.2. We use a reservoir compressibility of roughly 2×10^{-11} Pa^{-1} based on the formula $\kappa_C = 3/(4G)$ for an ellipsoidal reservoir and the earlier estimate of $G = 40\pm4$ GPa.

Magma Compressibility

Magma compressibility κ_M depends on gas volume fraction, solubility, crystallinity, and rate of loading. When changes in pressure are much more rapid than rates of gas exsolution (for example, the time scale of seismic-wave disturbances), the crystal, melt, and gas phases can be regarded as inert, and the bulk compressibility is simply the sum of the compressibilities of the crystal, melt, and gas phases (κ_x, κ_m, κ_g) multiplied by their respective volume fractions (v_x, v_m, v_g) (for example, Mastin, 2002):

$$\kappa_M = v_m\kappa_m + v_x\kappa_x + v_g\kappa_g . \quad (6)$$

If, on the other hand, pressure changes occur over months or years, as in the current eruption, gas exsolution must be considered. Previous investigators (Tait and others, 1989; Huppert and Woods, 2002; Woods and Huppert, 2003) used a simple Henry's solubility law for H_2O and found an abrupt discontinuity in compressibility at the saturation pressure (~240 MPa in fig. 6*C*). Huppert and Woods (2002) and Woods and Huppert (2003) suggested that this discontinuity could have a dramatic, rejuvenating effect on the course of an effusive eruption once the magma reservoir reaches the saturation pressure.

The Mount St. Helens magma contains both H_2O and CO_2, and gas in such a two-component system should exsolve more gradually and over a wider range of pressures than it would if only H_2O were present. We estimate exsolved volatile content and magma compressibility using petrologic constraints from other studies. Phase equilibrium experiments (Rutherford and Devine, this volume, chap. 31) suggest that the currently erupting magma last equilibrated at a temperature of ~850°C, a pressure of ~120 MPa, and a source depth near 5 km. The crystallinity at this depth was 40 to 55 percent (Pallister and others, this volume, chap. 30). The center of deflation, however, is substantially deeper than 5 km, perhaps equal to that of the May 18, 1980, magma at around 8–9 km depth and 220 MPa pressure (Rutherford and Devine, 1988). Following Gerlach and others (this volume, chap. 26), we assume that present-day magma properties at the source resemble those in 1980, with a temperature of about 900°C, pressure of ~220 MPa, 30 percent crystals (Cashman and Taggart, 1983), and

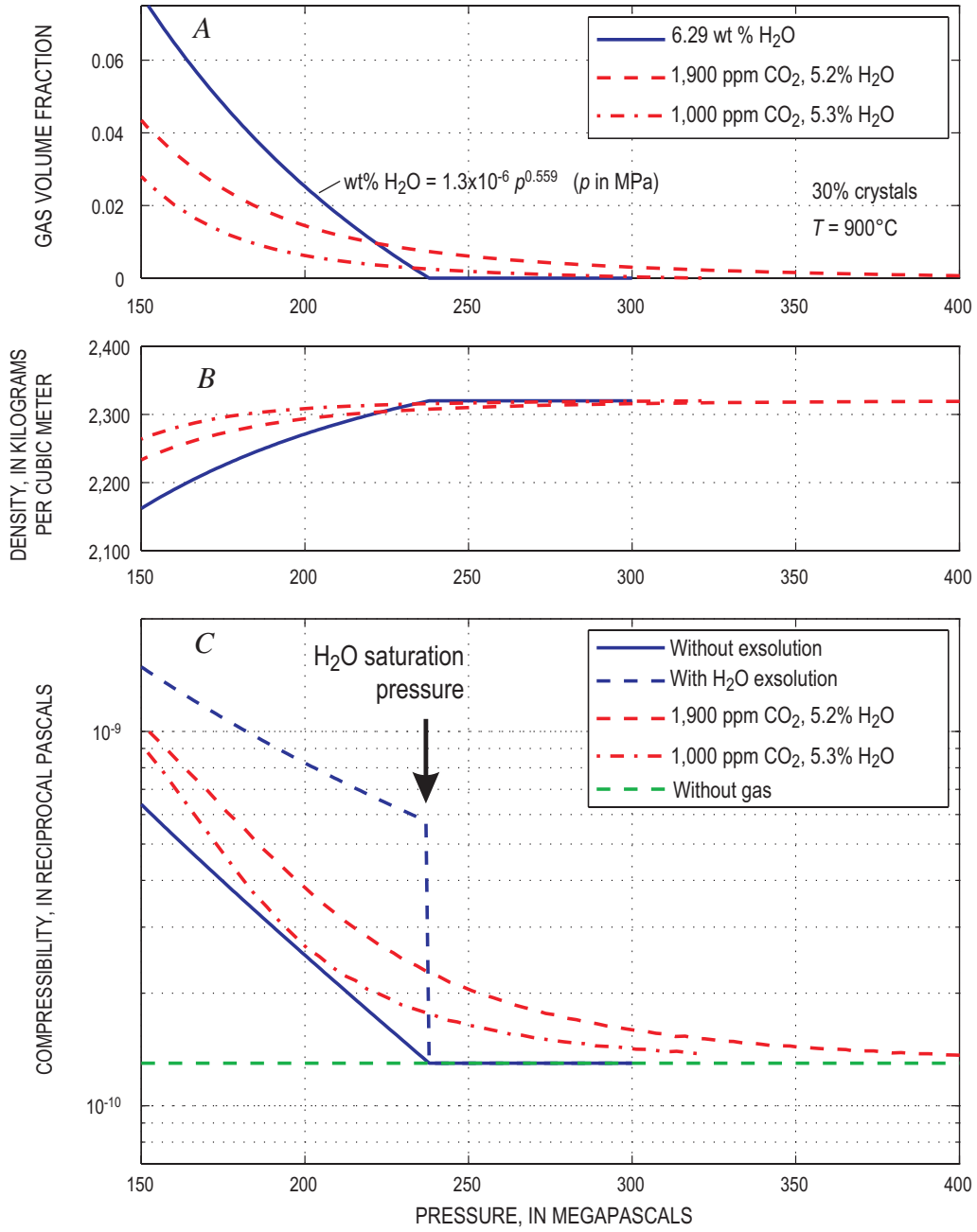

Figure 6. Characteristic features of magma having composition given in text, as function of pressure. Significance of the various lines is explained in text. *A*, Gas fraction by volume. *B*, Density. *C*, Compressibility.

a dissolved water concentration in the melt of about 5 weight percent (Blundy and Cashman, 2001).

Assuming that the CO_2 emitted into the atmosphere during this eruption originated from a mass of magma equal to that of the lava dome, Gerlach and others (this volume, chap. 26) estimate a preeruptive CO_2 concentration in the magma of about 1,100 ppm, or 1,900 ppm normalized to the melt alone (assuming 30 percent crystallinity). At 220 MPa pressure and 900°C temperature, with 5 weight percent dissolved H_2O, such a melt would contain roughly 350 ppm dissolved CO_2; the remaining CO_2 and H_2O would be exsolved in bubbles composing roughly 1.2 volume percent of the magma (Gerlach and others, this volume, chap. 26). The total water content normalized to the melt plus fluid phases would be about 5.2 weight percent.

Using the solubility code VolatileCalc 1.1 (Newman and Lowenstern, 2002), we calculate mass fractions of exsolved H_2O and CO_2 over pressures ranging from 150 to 400 MPa, and we combine these results with ideal gas relations to obtain the volume fraction of exsolved gas (fig. 6*A*). We assume a melt density $\rho_m = 2{,}200$ kg/m^3 and crystal density $\rho_x = 2{,}600$ kg/m^3; the melt density corresponds to a water-saturated melt of 1980

composition (sample SH-084 of Rutherford and others, 1985), calculated by the method of Ghiorso and Sack (1995) using the program Conflow (Mastin, 2002). From these volume fractions and phase densities we calculate the bulk density over the pressure range 150–400 MPa (fig. 6*B*) and then numerically calculate $(1/\rho_M)(\partial\rho_M/\partial p)$ to obtain κ_M (fig. 6*C*). We use a melt compressibility of 2.0×10^{-10} Pa^{-1}, estimated using the method of Ghiorso and Sack (1995) for water-saturated rhyolite at $p=220$ MPa, and a crystal compressibility of 2×10^{-11} Pa^{-1} obtained for albite at $T=900$°C and $p=220$ MPa from the program MELTS using the method of Elkins and Grove (1990).

Our calculations suggest that, over the pressure range of 150–400 MPa, the magma may have a bubble volume fraction of 0.0008 to 0.048 (fig. 6*A*). For comparison, we plot results for $CO_2=1{,}000$ ppm and $H_2O=5.3$ weight percent of the melt+fluid phases and also for a single-component (H_2O) volatile system using the Henry's law solubility illustrated in figure 6*A*, with the H_2O content (6.29 weight percent) set so that the volume fraction of gas at 220 MPa equals that of the two-component system. Both the two-component and the Henry's solubility laws show nearly an order-of-magnitude variation in compressibility over this pressure range, but the two-component systems show little or no discontinuity in κ_M at the saturation pressure. At $p=220$ MPa, the two-component system (1,900 ppm CO_2, 5.2 weight percent H_2O) gives $\kappa_M=2.8\times10^{-10}$ Pa^{-1}. We use this number as a starting point in our calculations. The relation between κ_M and volume fraction of gas for these two-component magma compositions is illustrated in figure 7.

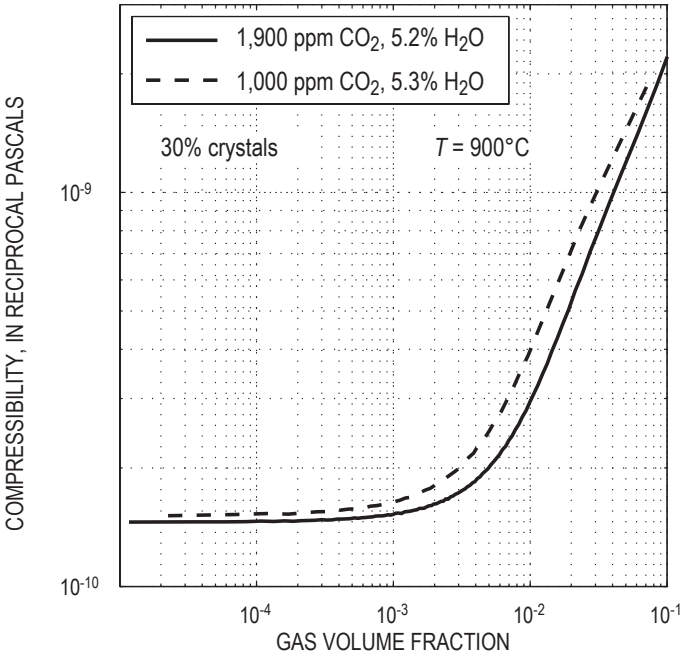

Figure 7. Compressibility versus volume fraction gas for a rhyolitic melt containing 30 percent crystals at 900°C temperature, using two different gas compositions.

Expected Ratio of Erupted Volume to Volume Change in the Reservoir

Using $\rho_M/\rho_e=1$, $\kappa_C=2\times10^{-11}$ Pa^{-1}, and $\kappa_M=2.8\times10^{-10}$ Pa^{-1} (~1.2 percent bubbles), then dV_e/dV_C predicted by equation 5 should be about 16, which is somewhat higher than the ranges of 7.7–12.8 and 2–6 calculated for the first and second time windows, respectively. A temporal increase in κ_M is suggested by the difference in apparent values of dV_e/dV_C between the first and second time windows, though uncertainties in these ratios are too great to make such an inference with confidence. For the overall eruption, the erupted volume by mid-December 2005, 7.3×10^7 m^3, was only about three times the reasonably well-constrained reservoir shrinkage dV_C of ~2.3×10^7 m^3 estimated by Lisowski and others (this volume, chap. 15). A ratio this low suggests a magma compressibility of ~4×10^{-11} Pa^{-1}, which is about one-fourth that of even a bubble-free magma of this crystallinity (fig. 7). If the magma reservoir is in fact bubble free, κ_C must be ~8×10^{-11} Pa^{-1} in order to have $dV_e/dV_C\approx3$; if it contains roughly 1 volume percent bubbles at the source depth, as inferred by Gerlach and others (this volume, chap. 26), κ_C must be ~1.4×10^{-10} Pa^{-1}. In either case, κ_M is only a few to several times greater than κ_C, which we take to indicate that the volume fraction of bubbles in the reservoir is zero or very small, consistent with the findings of Gerlach and others (this volume, chap. 26). If the reservoir was partially recharged during the eruption (a factor we consider later), a still lower ratio of κ_M/κ_C would be implied, suggesting still lower bubble content in the reservoir.

Idealized Models for History of Extrusion and Deflation

Previous studies (Wadge, 1981; Stasiuk and others, 1993; Huppert and Woods, 2002) point out that drainage of an elastic magma reservoir through a Newtonian conduit results in an exponentially decreasing extrusion rate. When combined with constant recharge rate into the magma system, the resulting curve has the form of an exponentially decreasing rate superimposed on a constant rate (fig. 3*D*). If these processes are responsible for determining the dome-growth curve at Mount St. Helens, then some information on the magma reservoir and conduit properties should be embedded in the coefficients to these equations. Information on the magma-reservoir volume and driving pressure are of particular importance.

We know that processes besides Newtonian flow and elastic relaxation may affect the growth history. The highly crystalline magma at Mount St. Helens, for example, probably has a non-Newtonian rheology. The extrusion of lava as a nearly solid plug bounded by frictional faults may also limit the growth rate. Different constitutive laws may predict dif-

ferent growth curves for the lava dome. Some curves fit to the hot-rock data (fig. 3) that have simple analytical forms are:

logarithmic (fig. 3*A*) $V_e = a\ln\left(1+b\left(t-c\right)\right)$, (7)

exponential (fig. 3*C*) $V_e = a\left(1-\mathrm{e}^{-b(t-c)}\right)$, (8)

modified log (fig. 3*B*) $V_e = a\ln\left[1-\frac{d}{b}\left(1-e^{\frac{b(t-c)}{a}}\right)\right]$, (9)

and exponential plus linear (fig. *3D*)

$$V_e = a\left(1-e^{-b(t-c)}\right)+d\left(t-c\right). \quad (10)$$

The terms *a*, *b*, *c,* and *d* are fitting coefficients; their best-fit values are listed in table 2. (Parameter *c*, which represents the day of the eruption start, is used as a variable in these fits, even though its value is roughly known, making the number of truly unknown parameters equal to three.) Curve forms that fit the data best are equations 9 and 10, which, as shown later, assume a constant rate of recharge. The fitting errors are lower using these forms than using equations 7 and 8 (table 2). More importantly, however, curves of equations 9 and 10 have done a better job predicting future growth, as the best-fit coefficients for equations 9 and 10 have changed relatively little since early 2005 (table 2).

Exponential Growth Curve

Exponential curve forms of equations 8 and 10 are derived from two main assumptions. The first is that the magma-reservoir pressure p is linearly related to the mass of magma in the reservoir:

$$p = p_0 - \mathrm{C}\left(M_e - M_i\right), \quad (11)$$

where M_e is the mass that leaves the reservoir (assumed to equal the erupted mass), M_i is the mass that enters the reservoir as recharge, p_0 is initial reservoir pressure, and C is a constant that represents the change in pressure with reservoir mass, $\partial p/\partial M_C$. By substituting equations 2 and 1 into equation 3, and rearranging, we find that $\mathrm{C} = [(\kappa_C+\kappa_M)\rho_m V_C]^{-1}$.

The second assumption is that the mass effusion rate $\dot{M}_e$ is linearly related to magma reservoir pressure (p):

$$\dot{M}_e = \mathrm{A}p - \mathrm{B}, \quad (12)$$

where A and B are constants. This equation describes, among other possibilities, Newtonian (Poiseuille) flow (fig. 8*A*); Newtonian flow capped by a frictional plug (fig. 8*C*); flow of a solid mass through the conduit separated from the conduit walls by a Newtonian fluid (a "greased plug"; fig. 8*B*); and

Table 2. Fitting coefficients to curves in figure 3.

[Columns labeled $\Sigma(y_i-y)^2$ give the sum of the squares of errors between best-fit predictions and data.]

Date	Days since 10/1/04	Hot-rock volume $m^3\times10^6$	Rate m^3/s	Exponential best-fit parameters								Logarithmic best-fit parameters							
				With recharge				Without recharge				With recharge				Without recharge			
				a $m^3\times10^6$	*b* $s^{-1}\times10^{-7}$	*c* s×10^5	*d* m^3/s	$\Sigma(y_i-y)^2$ $m^3\times10^{11}$	*a* $m^3\times10^6$	*b* $s^{-1}\times10^{-7}$	*c* s×10^5	$\Sigma(y_i-y)^2$ $m^3\times10^{11}$	*a* $m^3\times10^6$	*b* m^3/s	*c* s×10^5	*d* m^3/s	$\Sigma(y_i-y)^2$ $m^3\times10^{11}$	*a* $m^3\times10^6$	*b* $s^{-1}\times10^{-7}$	*c* s×10^5	$\Sigma(y_i-y)^2$ $m^3\times10^{11}$
10/1/04	0	0																			
10/13/04	12	5.4																			
11/4/04	34	11.8	5.92																		
11/29/04	59	21.3	4.4																		
12/11/04	71	25.5	4.05	14.0	2.94	9.56	2.79	0.31	53.8	1.23	9.49	0.75	8.0	3.81	9.70	8.28	0.21	39.5	1.74	9.55	0.4
1/3/05	94	30.5	2.52	86.7	1.01	9.61	-1.98	1.76	46.7	1.49	9.66	2.27	29.7	1.47×10^{-7}	9.71	7.55	2.42	29.5	2.58	9.75	4.8
2/1/05	123	35.1	1.84	94.3	0.96	9.59	-2.26	1.74	45.0	1.58	9.74	2.94	24.2	2.20×10^{-7}	9.88	8.34	3.31	24.5	3.40	9.94	13.5
2/21/05	143	39.2	2.37	28.1	2.19	9.76	1.15	10.16	48.2	1.41	9.49	13.24	24.6	1.40×10^{-7}	10.00	8.36	11.77	25.3	3.24	9.90	14.4
3/10/05	160	41.9	1.84	23.6	2.55	9.81	1.48	11.81	50.7	1.29	9.22	24.36	25.8	1.82×10^{-7}	10.04	8.11	15.17	25.9	3.12	9.86	15.5
4/19/05	200	47.5	1.62	22.9	2.63	9.82	1.52	11.87	55.4	1.10	8.43	57.96	22.2	0.52	9.87	8.28	17.58	26.9	2.92	9.74	18.7
6/15/05	257	53.9	1.3	25.7	2.32	9.72	1.35	14.62	61.1	0.92	7.16	107.49	21.9	0.56	9.87	8.31	17.62	27.8	2.75	9.61	21.8
7/14/05	286	57.1	1.28	26.4	2.25	9.67	1.31	15.41	64.5	0.83	6.31	143.93	21.3	0.63	9.88	8.38	17.93	28.6	2.61	9.47	21.8
8/10/05	313	61.7	1.97	24.9	2.42	9.79	1.39	23.82	69.3	0.73	4.96	253.01	18.1	0.96	9.98	8.92	39.02	30.8	2.29	9.02	77.1
10/24/05	388	70.0	1.28	25.0	2.41	9.77	1.38	23.86	78.3	0.57	1.65	485.74	16.2	1.13	10.06	9.44	51.27	34.4	1.87	7.98	179.4
12/15/05	440	73.0	0.67	27.7	2.06	9.40	1.26	71.01	82.9	0.51	-0.16	551.65	18.0	0.98	9.96	8.89	61.32	35.7	1.75	7.54	195.1

greased-plug flow capped by a frictional plug (fig. 8*D*). We also assume that the linear relations in equations 11 and 12 do not change with time.

If one further assumes that the rate of mass recharge $\left(\dot{M}_i = Q_i\right)$ is constant, equations 11 and 12 can be combined and integrated (appendix 2) to give the erupted mass as a function of time. Noting that the erupted volume (V_e) is equal to M_e/ρ_e, we obtain:

$$V_e = \frac{1}{\rho_e}\frac{\left(\mathrm{A}p_0 - \mathrm{B}\right) - Q_i}{\mathrm{AC}}\left(1 - e^{-ACt}\right) + \frac{Q_i}{\rho_e}t\,. \qquad (13)$$

This equation has the same form as equation 10 with the following coefficients:

$$a = \frac{\left(\mathrm{A}p_0 - \mathrm{B}\right) - Q_i}{\rho_e \mathrm{AC}}\,, \qquad (14)$$

$$b = \mathrm{AC}\,, \text{ and} \qquad (15)$$

$$d = \frac{Q_i}{\rho_e}\,. \qquad (16)$$

Differentiating equation 13 with respect to time, we find that this curve has an initial volumetric extrusion rate $\dot{V}_e^{t=0} = ab + d = (\mathrm{A}p_0 - \mathrm{B})/\rho_e$ but asymptotically approaches a linear trend having the slope $V_e^{t\to\infty} = d = Q_i/\rho_e$. Best-fit values of *a*, *b*, and *d* for the growth curve (table 2) suggest that $\dot{V}_e^{t=0} = \sim 7.0$ m^3/s (605,000 m^3/day) and $V_e^{t\to\infty} = \sim 1.26$ m^3/s (109,000 m^3/day). The latter value (the recharge rate) is several times greater than the long-term magma-supply rate of 0.2 m^3/s at Mount St. Helens, estimated by assuming that most of the volume of the edifice (~25 km^3) was erupted in the past 4,000 years (Iverson and others, 2006). Finally, the volume constant *a*, roughly 2.8×10^7 m^3, is the y-intercept of the long-term growth line in fig. 3*D* (the black dashed line). The y-intercept represents the volume of magma that has erupted and has not been replaced in the reservoir by recharge. The remaining volume, more than 4.5×10^7 m^3, represents recharge.

The physical significance of terms in *a* and *b* can be further refined, depending on the type of flow in the conduit. For Poiseuille flow, the mass flow rate is (Mironer, 1979, p. 194):

$$\frac{dM_e}{dt} = \frac{\rho_e \pi R^4}{8\eta H}\left(p - \overline{\rho} gH\right), \qquad (17)$$

where *H* is the conduit length, η is the average viscosity, and $\overline{\rho}$ is the average magma density between the magma reservoir and the Earth's surface. This equation assumes that the pressure at the top of the conduit is negligible (an assumption we will evaluate later). For Poiseuille flow, the constants in equation 12 are $\mathrm{A} = \rho_e \pi R^4/(8\eta H)$ and $\mathrm{B} = \rho_e \pi R^4 \overline{\rho}\, g/(8\eta)$. Inserting these expressions into equation 13, we can recast *a* in the following form:

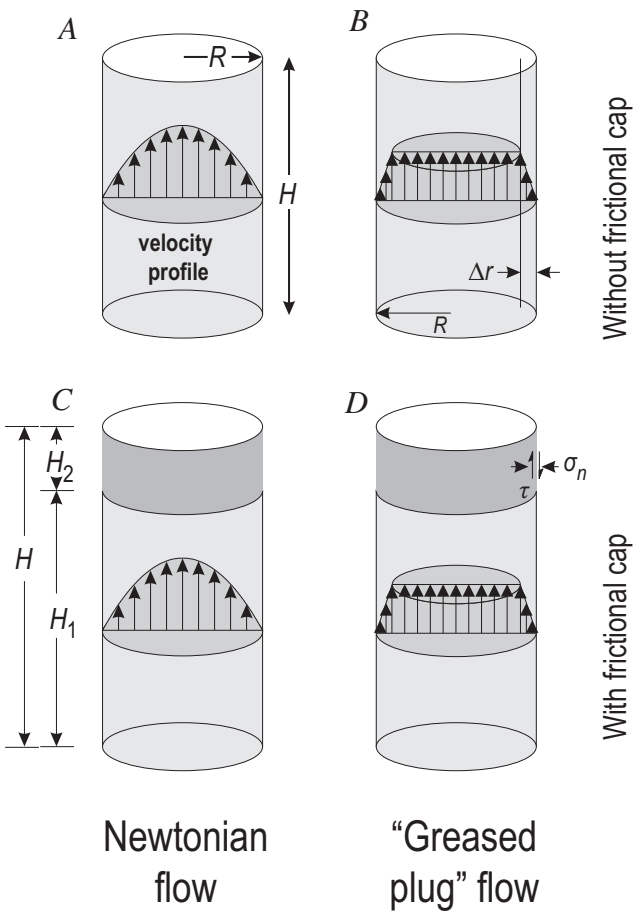

Figure 8. Types of conduit flow that are considered in deriving theoretical lava-dome growth curves. See text for full explanation.

$$a = \frac{\rho_M}{\rho_e}\left(\frac{\dot{V}_e^{t=0} - \dot{V}_e^{t\to\infty}}{\dot{V}_e^{t=0}}\right)\left(\kappa_C + \kappa_M\right)V_C\left(p_0 - \overline{\rho} gH\right). \qquad (18)$$

Equation (18) can be generalized by noting that $\left(p_0 - \overline{\rho} gH\right)$ is the initial pressure at the base of the conduit in excess of that required to initiate upward flow. Denoting this term as p_0^{ex}, we can rewrite the equations as:

$$a = \frac{\rho_M}{\rho_e}\left(\frac{\dot{V}_e^{t=0} - \dot{V}_e^{t\to\infty}}{\dot{V}_e^{t=0}}\right)\left(\kappa_C + \kappa_M\right)V_C p_0^{ex}\,, \qquad (19)$$

$$b = AC = \frac{\rho_e}{\rho_M}\frac{\dot{V}_e^{t=0}}{\left(\kappa_C + \kappa_M\right)V_C p_0^{ex}}\,. \qquad (20)$$

It can be shown (appendix 3) that these equations also apply to greased-plug flow (fig. 8*B*) and to flow of either a Newtonian

fluid or a greased plug capped by a frictional plug (figs. 8*C*, 8*D*; appendices 4, 5), so long as the plug's geometry and coefficient of friction do not change with time. If a frictional cap is present, p_0^{ex} represents the pressure in the magma reservoir in excess of both the pressure due to the weight of the overlying magma $(\overline{\rho} gH)$ and the pressure required to overcome frictional resistance of the plug.

Some important relations fall out of the equations above. In the absence of recharge, the final erupted volume is:

$$a = \frac{\rho_M}{\rho_e}(\kappa_C + \kappa_M)V_C p_0^{ex} \ . \qquad (21)$$

Using $\kappa_C = 8\times10^{-11}$ Pa^{-1}, $\rho_M / \rho_e \approx 1$, $V_C = 10$ km^3, $p_0^{ex} = \sim 30$ MPa, and $\kappa_M = 1.6\times10^{-10}$ Pa^{-1} appropriate for a bubble-free magma, the volume a is 7.2×10^7 m^3—roughly equal to the 7.3×10^7 m^3 that has erupted by the end of 2005. The time required for extrusion of 90 percent of this volume is about 3.5/b, or ~416 days. Using a magma compressibility consistent with 1 percent bubbles ($\kappa_M = 2.8\times10^{-10}$ Pa^{-1}) and $\kappa_C = 1.4\times10^{-10}$ Pa^{-1} (to maintain $dV_e / dV_C \approx 3$ following equation 5), we obtain a theoretical extrusion volume $a = 1.26\times10^8$ m^3 and duration of 2.0 years. These results suggest that the eruption could continue beyond early 2006 without recharge, but only if the exsolved volatile fraction in the reservoir is significantly greater than ~1 percent or if the reservoir is significantly larger than ~10 km^3, or both.

For the case of recharge, taking $\dot{V}_e^{t\to\infty} = 1.26$ m^3/s and $a = 2.8\times10^7$ m^3 (table 2), the product $V_C p_0^{ex}(\kappa_M + \kappa_C)$ obtained from equation 19 is about 3.4×10^7 Pa·m^3. Constraining the reservoir volume and initial overpressure requires some additional constraint on magma compressibility, which is considered later.

Friction, Faulting, and the Growth Curve

A log-based formula having the form of equations 7 or 9 would be predicted if the growth of the lava dome were controlled by frictional resistance of a solid mass in the upper conduit, with the coefficient of friction increasing with the rate of slip.

Although the coefficient of friction is commonly taken as a constant with a value of ~0.6–1.0 (Byerlee, 1978), it actually varies slightly with sliding rate and with time between sliding events (for example, Scholz, 1998). When μ increases with displacement rate, acceleration is dampened out and stable sliding (or fault creep) results. When μ decreases with displacement rate, sliding can accelerate unstably, leading to earthquakes. In general, rate-strengthening friction is favored when the shear-zone temperature is near the brittle-ductile transition (Chester, 1994), when a thick gouge layer is present (Byerlee and Summers, 1976), and in near-surface conditions when normal stress on the fault plane is low (Marone and Scholz, 1988). These conditions all exist in the shallow conduit at Mount St. Helens.

On the other hand, experimental studies of the Mount St. Helens fault gouge at 25°C (Moore and others, this volume, chap. 20) suggest rate-weakening behavior when displacement rates are less than about 1×10^{-4} m/s and rate-strengthening behavior at rates above 5×10^{-4} m/s. Assuming a 100-m-diameter conduit near the surface, the range of observed volumetric extrusion rates (~1–7 m^3/s) translates into displacement rates of $1–9\times10^{-4}$ m/s, crossing over the transition between these behavior types. We consider it likely that both rate-strengthening and rate-weakening sliding exist at shallow depth at any given time. Fault patches of rate-weakening gouge will slip abruptly to create small drumbeat earthquakes whereas other parts of the fault surface creep stably under rate-strengthening conditions. If rate-weakening behavior controls conduit flow, the appropriate friction coefficient to use in this model would be a value averaged over many stick-slip cycles. If that average doesn't change with time, the long-term growth curve will be exponential. But if rate-strengthening behavior controls conduit flow, we need to consider the stress-strain rate relations of rate-strengthening fault creep.

The Logarithmic Curve

When the coefficient of friction is rate-dependent, the shear stress that resists slip on a fault plane is commonly expressed as (for example, Scholz, 1998):

$$\tau = \tau_o + A_1 \sigma_n \ln \frac{\dot{\delta}}{\dot{\delta}_o}. \qquad (22)$$

Here σ_n is normal stress at the wall and A_1 is the rate dependence of fault strength. The constant τ_o is an arbitrary reference, the strength of the wall interface when the slip rate is $\dot{\delta}_o$.

In order to derive a growth curve, we assume that the frictional plug of mass M_p and length H_2 occupies a cylindrical conduit of radius R (fig. 8*C*). The frictional force along the plug margin is $2\pi R H_2 \mu \overline{\sigma}_n$, where $\overline{\sigma}_n$ is the mean normal stress on the plug margin. The mass flow rate $\dot{M}_e$ is then related to $\dot{\delta}_o$ by $\dot{M}_e = \rho_e \pi R^2 \dot{\delta}$, and pressure at the plug base (p) is related to mass flow rate as:

$$p = p_o + a \ln \frac{\dot{M}_e}{\dot{M}_o}, \qquad (23)$$

where $a = 2A_1 \overline{\sigma}_n H_2 / R$ and $p_0 = 2\tau_0 H_2 / R + Mg / \pi R^2$ are constants.

Rearranging this equation yields:

$$\dot{M}_e = e^{\dot{M}_0} \exp\left[\frac{(p - p_o)}{a}\right]. \qquad (24)$$

Combining equation 24 with equation 11 (assuming recharge $M_i = 0$) and integrating leads to (appendix 6):

$$V_e = aD \ln\left(1 + \frac{t\dot{M}_0}{\rho_e D a}\right), \qquad (25)$$

where $D = V_M\left(\kappa_C + \kappa_M\right)$ and V_M is the volume of the magma reservoir plus conduit. This equation has the same form as equation 7, with $a = \alpha V_M\left(\kappa_C + \kappa_M\right)$ and $b = \dot{V}_e^{t=0}/a$.

If recharge into the magma reservoir is included, the equation has the form (appendix 6):

$$V_e = \alpha D \ln\left[1 - \frac{\dot{M}_0}{Q_i}\left(1 - e^{\frac{Q_i t}{\rho_e \alpha D}}\right)\right]. \qquad (26)$$

This equation has the form of equation 10, with a volume constant $a = \alpha D = 1.47\times10^7$ m^3 (by regression through the most recent data set, table 2), a recharge rate $b = Q_i/\rho_e = 1.0$ m^3/s, and an initial extrusion rate $d = \dot{M}_0/\rho_e = \dot{V}_e^{t=0} = 8.9$ m^3/s (table 3). The recharge rate is about 30 percent less than the 1.26 m^3/s obtained from the exponential curve. By rearranging equation 23, substituting $\dot{M}_e = \rho_e \dot{V}_e$, $\dot{M}_0 = \rho_e \dot{V}_e^{t=0}$, and $a = \alpha D = \alpha V_M(\kappa_C + \kappa_M)$, we can obtain a formula for the product of volume of the magma system and pressure drop from the beginning of the eruption until the time of the last data point used in this paper (December 15, 2005):

$$V_M \Delta p\left(\kappa_C + \kappa_M\right) = a \ln\left(\dot{V}_e^{t=0}/\dot{V}_e^{last}\right). \qquad (27)$$

The parameters Δp and $\dot{V}_e^{last}$ are the pressure change at the base of the frictional plug and the extrusion rate at the end of this time period; the variable a is the numerical value of the fitting coefficient. From the first derivative of equation 9, $\dot{V}_e^{last} = 1.20$ m^3/s as of December 15, 2005 (table 3), giving $V_M \Delta p\left(\kappa_C + \kappa_M\right) = 3.0\times10^7$ m^3. It should be noted that this term contains slightly different parameters from $V_C p_0^{ex}\left(\kappa_C + \kappa_M\right)$ derived for the exponential curve: V_C represents reservoir volume, whereas V_M represents volume of the reservoir plus conduit below the frictional plug, and Δp represents pressure drop at the base of the plug, whereas p_0^{ex} gives the initial overpressure in the magma reservoir. Nevertheless, the values of these terms should be roughly comparable, and they are: $V_M \Delta p\left(\kappa_C + \kappa_M\right) = 3.0\times10^7$ m^3 from the log fit (equation 9) versus $V_C p_0^{ex}\left(\kappa_C + \kappa_M\right) = 3.4\times10^7$ m^3 from the exponential fit (equation 10). The fact that these values differ by only 10 to 15 percent suggests that inferences about magma-reservoir size and overpressure do not depend strongly on the assumptions regarding factors that control conduit flow.

Additional Constraints from the Geodetic Time Series

On the basis of their fit to the dome-growth data, neither the logarithmic (equation 9) nor the exponential (equation 10) model can be confidently eliminated. Each, however, predicts a history of reservoir deflation that can be compared with geodetic data. For the case of exponential dome growth, differentiating equation 13 with time under conditions of constant recharge and substituting in equations 4, 14, and 15 gives the following for reservoir deflation with time:

$$\Delta V_C = -\frac{\rho_e}{\rho_M}\frac{a\left(1 - e^{-bt}\right)}{\left(1 + \frac{\kappa_M}{\kappa_C}\right)}. \qquad (28)$$

The reservoir deflates with the same time constant as the dome-growth curve, implying, for the best-fit value of b with recharge through December 15, 2005 (2.06×10^{-7} s^{-1}), that 90 percent of the geodetic deflation should have occurred after about 200 days, by mid-April 2005, and that by late summer 2005 the deflation should have essentially stopped. This is inconsistent with geodetic data, which show a nearly linear rate of inward displacement through at least the end of 2005. The log curve can theoretically provide a better match to the geodetic data, but the predictions at some point become physically unrealistic. For the case of zero recharge, for

Table 3. Calculations of $V_C p_0^{ex}(\kappa_M+\kappa_C)$ or $V_M\Delta p(\kappa_M+\kappa_C)$ obtained from exponential or logarithmic best-fit solutions.

Date	$V_C p_0^{ex}(\kappa_M+\kappa_C)$ exponential		Log with recharge			Log without recharge		
	With recharge m$^3\times10^6$	Without recharge m$^3\times10^6$	$\dot{V}_e^{t=0}$ m^3/s	$\dot{V}_e^{last}$ m^3/s	$V_M\Delta p(\kappa_M+\kappa_C)$ m$^3\times10^6$	$\dot{V}_e^{t=0}$ m^3/s	$\dot{V}_e^{last}$ m^3/s	$V_M\Delta p(\kappa_M+\kappa_C)$ m$^3\times10^6$
12/11/2004	24	54	8.3	3.94	5.9	6.9	3.4	28
1/3/2005	67	47	7.5	2.52	33	7.6	2.5	33
2/1/2005	71	45	8.3	1.82	37	8.3	1.8	37
2/21/2005	33	48	8.4	1.64	40	8.2	1.7	40
3/10/2005	29	51	8.1	1.54	43	8.1	1.5	43
4/19/2005	29	55	8.3	1.40	39	7.8	1.3	48
6/15/2005	31	61	8.3	1.20	42	7.6	1.1	54
7/14/2005	32	64	8.4	1.14	42	7.5	1.0	57
8/10/2005	31	69	8.9	1.23	36	7.1	1.0	61
10/24/2005	31	78	9.4	1.24	33	6.4	0.9	68
12/15/2005	34	83	8.9	1.11	38	6.2	0.8	72

example, combining equations 5 and 25 and substituting $a = \alpha V_C (\kappa_C + \kappa_M)$ and $b = \dot{V}_e^{t=0} / a$, the volume shrinkage of the magma system should follow the curve:

$$\Delta V_C = -\frac{\rho_e a \ln(1+bt)}{\rho_M \left(1+\frac{\kappa_M}{\kappa_C}\right)} . \qquad (29)$$

In other words, the volume shrinkage of the magma reservoir with time should look like a negative mirror image of the dome growth curve, adjusted by the constant $\rho_e/(\rho_M(1+\kappa_M/\kappa_C))$. This curve leads to the physically unrealistic result that deflation continues indefinitely, even to negative reservoir volumes, at the same time that the lava dome keeps growing. This implication is an outcome of the logarithmic relation between stress and displacement rate (equation 22), which adequately fits experimental data on rate-dependent friction within the range of shear stresses applied during experiments but cannot be realistically extrapolated outside that range.

A More Realistic Model

We are therefore left with the result that neither the exponential curve nor the logarithmic curve can adequately fit both the lava-dome growth curve and the geodetic deflation history. What additional processes might account for the dome growth and deflation histories? Some possibilities include:

- *The effect of the dome's weight in suppressing further extrusion.*—Digital elevation models indicate that the dome rapidly grew to more than 200 m height in the first two months of the eruption, potentially adding several megapascals of increased pressure to the vent at the base of the dome. Our records on dome-height variations with time (fig. 9) can be used to constrain this effect.
- *Changes in magma compressibility with time.*—A decrease in reservoir pressure of 30 MPa can increase magma compressibility several tens of percent (fig. 6*C*), increasing the ability of the magma reservoir to maintain a long-term eruption with time.
- *A nonconstant rate of recharge.*—A more realistic model would have recharge into the reservoir increasing as reservoir pressure decreases.

These effects require a numerical solution to account for changing values with time. We solve the problem using differential equations described below.

To account for the relation between mass eruption rate and reservoir pressure, we assume again that the effusion rate is linearly related to the reservoir overpressure. For Poiseuille or greased-plug flow, the overpressure p^{ex} is simply $p - \bar{\rho} g H$. If a frictional cap is present, the overpressure is $p^{ex} = p - (\bar{\rho} g H + F)$, where F is the strength of the frictional cap (assumed constant). The growth of the lava dome changes the distance H from the reservoir to the free surface, and in order to account for this, we divide this term into two parts; $\bar{\rho} g H_0$, where H_0 is the distance from the top of the reservoir to the vent at the base of the lava dome, and $\rho_e g H_3$, where H_3 is the height of the lava dome. The relation between pressure and effusion rate is then:

$$\frac{dM_e}{dt} = \mathrm{A}_2 \left[\frac{p - (\bar{\rho} g H_0 + \rho_e g H_3 + F)}{H_0 + H_3} \right] . \qquad (30)$$

The constant A_2 has the value $\rho_e \pi R^4/(8\eta)$ for Poiseuille flow and $\rho_e \pi R^3 \Delta r/(8\eta)$ for greased-plug flow (appendix 4). This

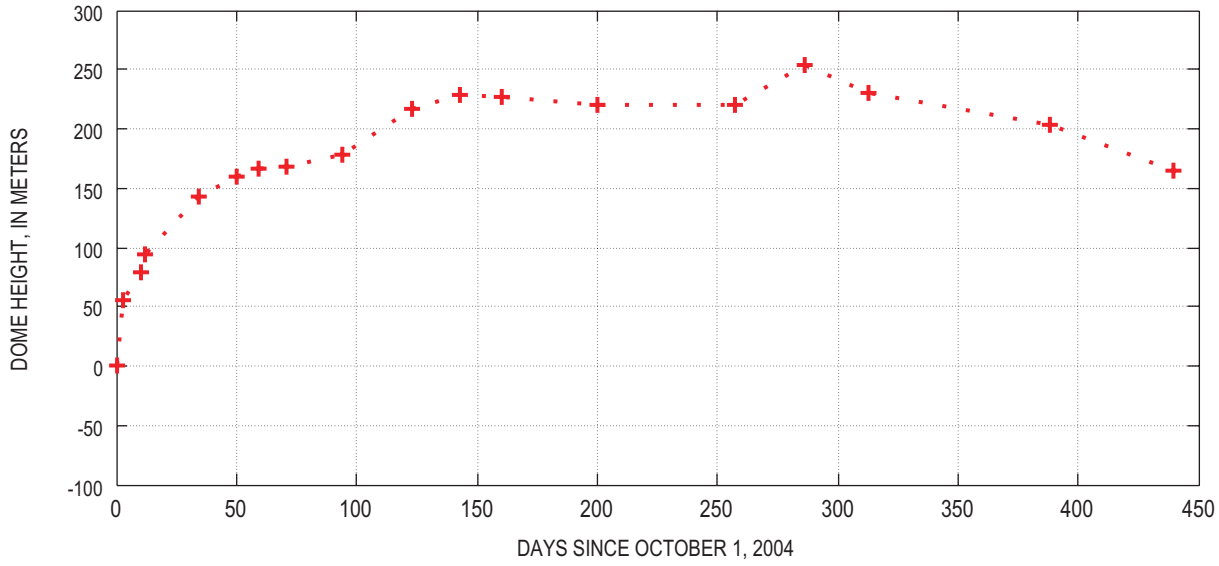

Figure 9. Maximum height of the Mount St. Helens lava dome above the 2003 crater floor (the Crater Glacier surface, approximately 2,115 m above sea level) during the course of the 2004–6 eruption.

equation can be simplified by noting that, at $t=0$, $p^{ex}=p_0^{ex}$ and $dM_e/dt = \dot{V}_e^{t=0}/\rho_e$:

$$\frac{dV_e}{dt} = \dot{V}_e^{t=0}\,\frac{p_0^{ex}+\Delta p-\rho_e g H_3}{p_0^{ex}} \quad . \tag{31}$$

The initial extrusion rate $\dot{V}_e^{t=0}$, the dome height H_3, and the density ρ_e are constrained from measurements; the pressure change in the magma reservoir Δp is calculated by integration (below); and the initial overpressure p_0^{ex} is an adjustable parameter whose value is likely less than a few tens of megapascals.

The rate of pressure change in the reservoir is obtained by differentiating equation 11 with time and substituting $C=[(\kappa_C+\kappa_M)\rho_m V_C]^{-1}$:

$$\frac{dp}{dt} = \frac{\dfrac{dM_i}{dt}-\rho_e\dfrac{dV_e}{dt}}{\rho_M V_C\left(\kappa_C+\kappa_M\right)} \quad . \tag{32}$$

In this calculation, the terms κ_C and ρ_e are considered known; dV_e/dt is obtained from equation 31, and the recharge rate dM_i/dt is calculated from a separate differential equation (below). The magma compressibility κ_M at the beginning of the eruption is an adjustable parameter; during the course of the eruption, it increases with decreasing pressure at a rate that equals the average slope of the curve of κ_M versus p in figure 6*C* (for CO_2=1,900 ppm, H_2O=5.2 weight percent). In each calculation, we use the magma density ρ_M shown in figure 6*B* at the given compressibility. Thus the magma density changes with pressure, though the changes are minor.

In accounting for recharge, we assume that the rate of input into the magma reservoir at the onset of the eruption was negligible but increased as reservoir pressure was depleted. The simplest such relation is linear, using an adjustable proportionality constant Q_{lt}:

$$\frac{dM_i}{dt} = -Q_{lt}\,\frac{\Delta p}{p_0^{ex}} \quad . \tag{33}$$

The parameter Δp is the reservoir-pressure change since the start of the eruption (negative Δp implies a pressure decrease). Like Q_i in equation 13, Q_{lt} in equation 33 largely controls the long-term extrusion rate. The linear assumption implies laminar flow of magma into the reservoir from some deeper source whose pressure remains constant. A more realistic model would consider a finite source whose pressure decreased over time, but we have no constraints on the rate of pressure decrease and hence ignore it under the assumption that the deeper reservoir is much larger than the shallow one that feeds the eruption.

Equations 31, 32, and 33 can be simultaneously integrated to yield both a dome-growth curve and deflation history. The calculations involve four adjustable constants: V_C, p_0^{ex}, an initial value of κ_M, and Q_{lt}. Our solution takes κ_C to be a known quantity, although its value is known only approximately. The above estimates of $V_e/\Delta V_C$ suggest κ_C to be at least a few times greater than our initial estimate of 2×10^{-11} Pa^{-1}, but best-fit values of $V_C p_0^{ex}\left(\kappa_C+\kappa_M\right)$ in table 3 constrain $\left(\kappa_C+\kappa_M\right)$ to be less than about 5×10^{-10} Pa^{-1} for magma-reservoir volumes greater than about 5 km^3 and initial overpressures exceeding about 10 MPa. With these constraints, we run the model using two possible values of 7×10^{-11} and 1.5×10^{-10} Pa^{-1} for κ_C. In theory, the values of Q_{lt} and κ_M can be uniquely determined, as they are the only factors that significantly affect the long-term eruption rate and the ratio $V_e/\Delta V_C$, respectively. The values of V_C and p_0^{ex} are interdependent and nonunique, but ranges of possible combinations can be identified.

In order to compare the deflation history to geodetic measurements, we convert the history of pressure change Δp into a history of magma-chamber shrinkage ΔV_C, using $\Delta V_C=(V_C/\kappa_C)\Delta p$, and then convert ΔV_C into a theoretical displacement at JRO1 using one of the geodetic models in table 1 (fig. 4). For the first time period (fig. 4*A*), model 5 in table 1 (source depth 6–10 km) matches the JRO1 radial displacements best and predicts a radial displacement of 5.32 mm for a volume loss ΔV_C of 3.85×10^6 m^3, or 1.4×10^{-6} mm displacement per cubic meter volume loss.

Results

Numerical model results are compared with measurement histories of lava-dome volume and radial displacement at JRO1 in figures 10*A* and 10*B*, respectively. The solid black line in fig. 10*A* gives model results that match the hot-rock data for V_C=17 km^3, p_0^{ex}=17 MPa, and Q_{lt}/ρ_e = 1.7 m^3/s. The dashed black line gives analytical results using the exponential curve of equation 10 with $a=2.77\times10^7$ m^3, $b=2.06\times10^{-7}$ s^{-1} and d=1.26 m^3/s. These theoretical curves cannot be easily compared with the JRO1 data because deflation at JRO1 began around September 23, 2004, 20 days before the first lava appeared and three days before the first visible surface deformation (Dzurisin and others, this volume, chap. 14). The deflation between September 26 and October 11 was probably associated with extrusion of cold rock ahead of the rising magma. Deflation before September 26 may have been associated with intrusion at shallow depth or gas escape, neither of which can be easily quantified.

In order to simultaneously fit both curves, we add the volume of cold rock extruded before October 11 to the cumulative hot-rock volume (green data points, fig. 10*A*) and use September 27 as the start date (a date determined by a best-fit exponential curve through these new data). We also start with 3 mm of deflation at $t=0$, the approximate amount of deflation measured at JRO1 on September 27.

The blue dashed and solid lines in figure 10*A* represent best-fit analytical (using equation 10) and numerical curves through the modified dataset, respectively. Best-fit coefficients of the analytical curve give $a=3.61\times10^7$ m^3, $b=2.2\times10^{-7}$ s^{-1}, and d=1.28 m^3/s. Using $\kappa_C=7\times10^{-11}$ Pa^{-1}, $\kappa_M=1.2\times10^{-10}$ Pa^{-1} (adjusted to match the deflation curve) and equation 28 to calculate magma-reservoir deflation with time, the calculated displacements (dashed blue line, fig. 10*B*) roughly match the measurements during the first few months of the eruption and

during the following summer (~250–400 days into the eruption), but they do not predict continued deflation that one would infer from a best-fit line through the JRO1 data after about 150 days.

A numerical solution (solid blue lines) provides a slightly better fit through the data using $V_C = 17$ km^3, $p_0^{ex} = 18$ MPa, $Q_{li}/\rho_e = 1.7$ m^3/s, and κ_M ranging from an initial value of 1.85×10^{-10} Pa^{-1} to a final value of 1.98×10^{-10} Pa^{-1} (~0.40–0.48 percent bubbles). In this solution, the total volume of erupted magma that has not been replaced by recharge is about 3.9×10^7 m^3. This amount is 1.3×10^7 m^3 less than predicted by the analytical solution (fig. 10*A*). The lower total recharge implies more geodetic deflation; hence the numerical curve can be fit to the geodetic data using a slightly higher average κ_M than required by the analytical solution. Over the time window of the simulation, the magma-reservoir pressure drops by about 11 MPa, so that the excess pressure $(p - \bar{\rho} g H_1)$ by mid-December 2005 is about 7 MPa, three megapascals greater than the pressure $\rho_e g H_3$ at the vent, owing to the weight of the overlying dome (taking $\rho_e = 2300$ kg/m^3 and $H_3 = 167$ m on December 15, 2005).

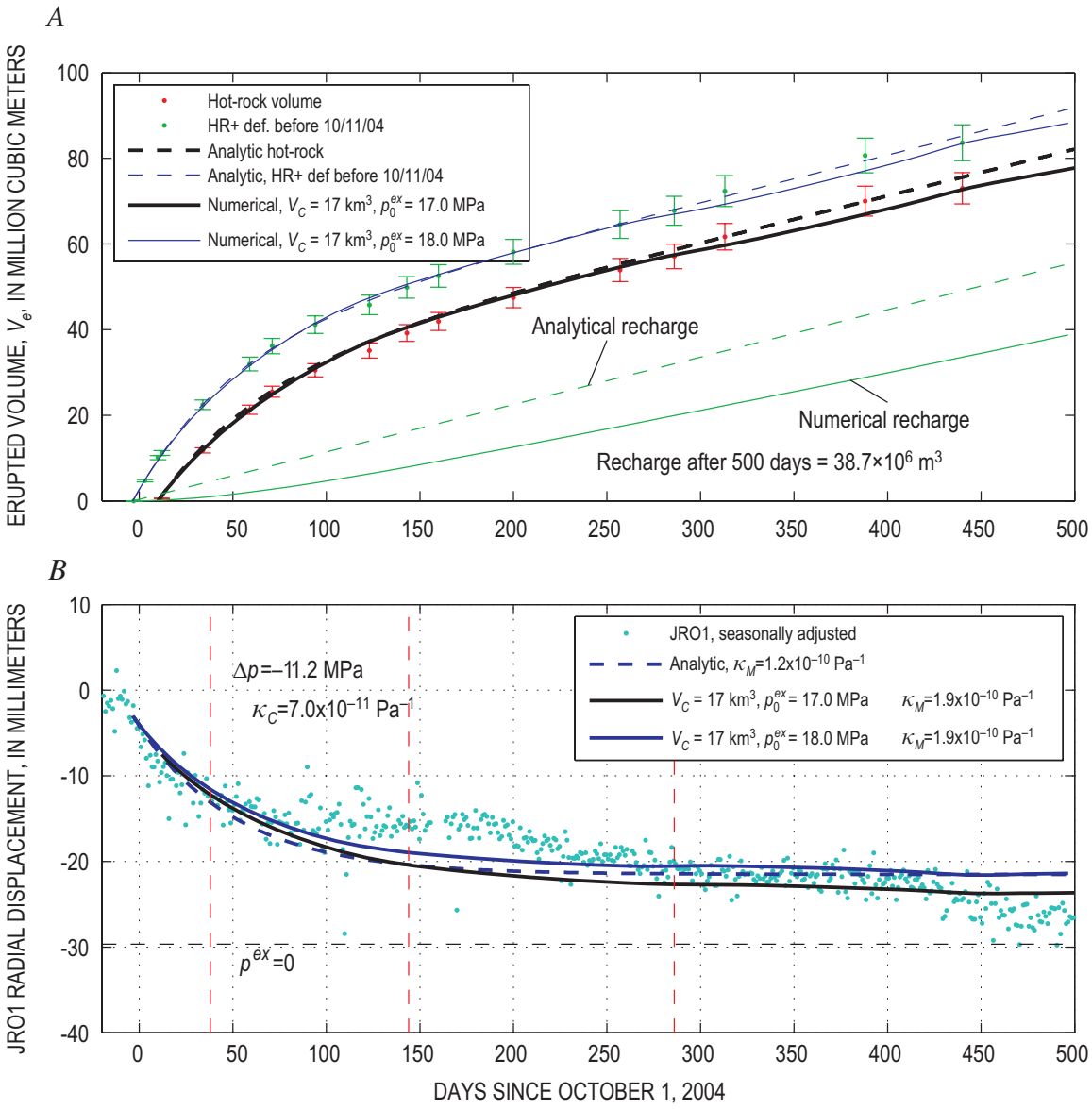

Figure 10. Comparison of theoretical and measured lava-dome volume and magma-reservoir deflation with time at Mount St. Helens. *A*, Erupted volume from digital elevation models. Phrase "HR+def before 10/11/04" refers to data points that represent hot-rock volume of the dome plus volume of uplifted cold crater-floor material that appears before the beginning of lava extrusion on October 11, 2004. Phrase "Analytic, HR+def before 10/11/04" refers to an analytical best-fit line through these data. Details are explained in text. *B*, Radial displacement measured at JRO1 continuous GPS station (fig 1*A*). Negative displacements are radially inward. Red vertical dashed lines in figure 10*B* refer to the start and end dates of time windows used in geodetic analysis (fig. 4 and table 1).

Other combinations of ΔV_C, p_0^{ex}, Q_{lt}, and κ_M that produce reasonable fits by numerical solution are listed in table 4. All combinations require $Q_{lt}/\rho_e = 1.7 \pm 0.1$ m^3/s. Runs that use $\kappa_C = 7\times10^{-11}$ Pa^{-1} require average values of κ_M around 1.6–1.9×10^{-10} Pa^{-1} (0.18–0.43 volume percent bubbles) and a magma-reservoir volume exceeding ~9 km^3 for p_0^{ex}<~30 MPa. Runs that use $\kappa_C = 15\times10^{-11}$ Pa^{-1} require $\kappa_M = 4.0$–4.7×10^{-10} Pa^{-1} (1.0–1.8 volume percent bubbles) and a magma-reservoir volume exceeding ~5 km^3 for p_0^{ex} less than about 30 MPa. Using a still larger reservoir compressibility ($\kappa_C = 3\times10^{-10}$ Pa^{-1}), a magma reservoir larger than 2 km^3 (for p_0^{ex} less than about 30 MPa) can still fit the curves using $\kappa_M = 8.9$–9.4×10^{-10} Pa^{-1} (2.8–3.8 percent bubbles). The results that involve $\kappa_C = 7$ to 15×10^{-11} Pa^{-1} correspond to exsolved fluid contents in the source region that match most closely with gas emission data (Gerlach and others, this volume, chap. 26).

Table 4. Combinations of V_C, p_0^{ex}, Q_{lt}, and average value of κ_M that yield reasonable fits to the growth curve and geodetic data by numerical calculation; also given are the pressure drop Δp in the magma reservoir and the recharge volume calculated after 500 days of eruption.

κ_C Pa^{-1}×10^{-11}	V_C km^3	p_0^{ex} MPa	avg κ_M Pa^{-1}×10^{-10}	Q_{lt}/ρ_e m^3/s	Δp MPa	Recharge m^3×10^6
7	6	41	1.6	1.7	-30.5	48.7
7	8	32	1.6	1.7	-23	46.7
7	10	27	1.8	1.7	-18.7	44.4
7	12	24	1.8	1.7	-16.3	42.9
7	14	21	1.9	1.7	-13.7	40.9
7	17	19	1.9	1.7	-12.0	39.0
7	20	16.5	1.9	1.7	-9.9	37.0
7	24	15	1.9	1.7	-8.6	34.9
7	27	14	1.9	1.7	-7.8	33.4
14	4	34	3.0	1.7	24.7	47.1
14	6	25	3.1	1.7	17.1	43.6
14	8	19	4.0	1.7	-12.0	39.2
14	10	16	4.1	1.7	-9.4	36.4
14	12	14.5	4.2	1.7	-8.2	34.2
14	14	13.3	4.2	1.7	-7.1	32.2
14	17	12	4.3	1.7	-6.0	29.6
14	20	11	4.7	1.7	-5.0	26.7
14	24	10.2	4.7	1.7	-4.3	24.3

The Quandary of Continued Deflation

Like the exponential function, the numerical solution predicts that deflation should have nearly ended several months after the eruption began, which does not agree with the geodetic data. Factors that might keep both the extrusion rate and the deflation rate more or less constant include (1) decreasing magma viscosity or friction coefficient with time; (2) increasing conduit diameter with time; and (or) (3) a nonlinear relation between extrusion rate and friction coefficient, similar to the logarithmic relation.

As of March 2006 there have been no obvious temporal changes in petrology or fault-gouge characteristics that might reflect changes in viscosity or friction coefficient (Pallister and others, this volume, chap. 30). Changes in conduit diameter cannot, however, be dismissed (our field observations are insufficient), nor can the possibility that conduit enlargement alone, in the absence of recharge, is responsible for sustained extrusion rates. Figure 11*B* shows a theoretical deflation curve calculated in the absence of recharge by solving equation 5 for reservoir volume loss dV_C using $(\rho_M/\rho_e) = 1$, $\kappa_M = 3.3\times10^{-10}$ Pa^{-1} (adjusted to optimize fit), $\kappa_C = 7\times10^{-11}$ Pa^{-1}, and the erupted volume dV_e ($= V_e$) obtained from the best-fit curve, equation 10, through modified hot-rock data (fig. 11*A*). The theoretical curve matches the long-term linear trend quite well but underestimates the deflation in the first few months of the eruption. The rapid early deflation implies that the volume removed from the reservoir per unit erupted volume was initially high but then decreased with time, a characteristic that could be explained by either increasing recharge or by increasing magma compressibility with time. Starting with a slightly lower compressibility (3.2×10^{-10} Pa^{-1}) that increases to 4.1×10^{-10} Pa^{-1} over the course of the eruption (fig. 11*B*, red dashed line) does not appear to reconcile the difference.

The pressure change Δp is related to the volume shrinkage dV_C by $\Delta p = dV_C/(V_C\kappa_C)$. For $V_C = 15$ km^3, for example, the deflation in figure 11*B* represents a pressure drop of about 15–16 MPa, requiring an initial overpressure above this value to sustain the eruption for the observed time period. The conduit radius R that could give the instantaneous growth rate in figure 11*A* with the pressure in figure 11*B* can be calculated from equation 17 by substituting $p_0^{ex} + \Delta p - \rho_e g H_3$ for $\left(p - \bar{\rho} g H\right)$, $\dot{V}_e^{t=0}$ for $\left(\pi R_0^4 p_0^{ex}/8\eta H\right)$, and $\rho_e \dot{V}_e$ for dM_e/dt:

$$R = R_0\left[\left(\frac{\dot{V}_e}{\dot{V}_e^{t=0}}\right)\left(\frac{p_0^{ex}}{p_0^{ex} + \Delta p - \rho_e g H_3}\right)\right]^{1/4}. \qquad (34)$$

Here, R_0 is the initial conduit radius. Calculating the change in R with time requires values of V_C and p_0^{ex} to be assumed in advance. For $V_C = 15$ km^3 and $p_0^{ex} = 30$ MPa, the observed extrusion history can be produced by a roughly 15-percent decrease in conduit radius in the first few months of the eruption, followed by widening at a slow but accelerating rate (fig. 11*C*). As the overpressure approaches zero, the conduit radius must approach infinity to keep the extrusion rate constant (for example, the line for $p_0^{ex} = 15$ MPa in fig. 11*C*).

These results suggest that the changes in conduit radius required to maintain the observed eruption rate without recharge are less than a few tens of percent and thus probably too small to be easily detected by observed variations in lithic content of the lava or ratios in linear to volumetric extrusion rate. The changes shown in figure 11, however, involve a seemingly unrealistic shrinkage in radius early in the eruption, when effusion rates are high, followed by enlargement at an accelerating rate when effusion rates are low. We cannot dismiss conduit-radius changes in the absence of recharge, but we

are inclined to consider them less likely than recharge-driven flow. Future developments may help distinguish these possibilities: If extrusion is sustained by conduit widening without recharge, geodetic deflation will continue and the eruption will eventually wane, then stop. If it is sustained by recharge, geodetic deflation will soon stabilize, but the eruption may continue for years and end gradually as the deeper magma source is depleted.

Finally, one explanation for continued deflation may lie in the results of the numerical models. Model runs using

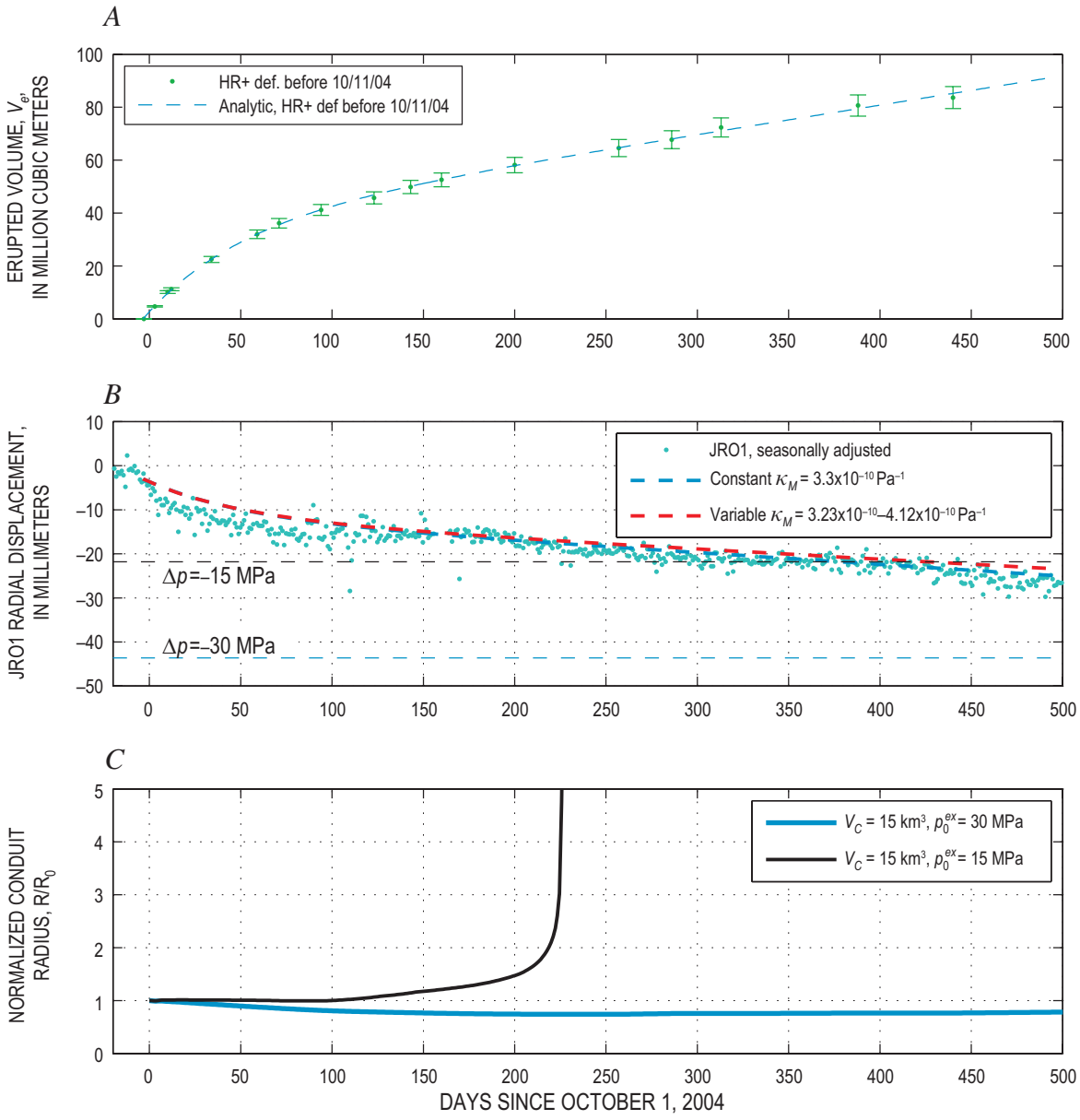

Figure 11. Modeled relation between extruded volume, magma pressure and overpressure, and conduit radius at Mount St. Helens. *A*, Erupted volume, V_e. Data points with error bars represent hot-rock volume of the lava dome plus volume of cold rock uplifted before October 11, 2004 (compare fig. 10*A*). Error bars are ±5 percent as in figures 2 and 10. *B*, Station JRO1 radial displacements (dots) compared with the displacements predicted at this point for deflation of a 15-km³ ellipsoidal magma body at 6–10 km depth with $\kappa_C = 7\times10^{-11}$ Pa⁻¹ and (1) a constant $\kappa_M = 3.3\times10^{-10}$ (blue dashed line) or (2) κ_M increasing from 3.2×10^{-10} to 4.2×10^{-10} as pressure drops by 15 MPa (dashed red line). Negative displacements are radially inward. *C*, Conduit radius, *R*, required to maintain extrusion rate illustrated in figure 11*A*, normalized to the initial conduit radius, R_0. Magma pressure is inferred from deflation curve, assuming an initial overpressure of 30 MPa (blue line) or 15 MPa (black line). Method of calculating pressure change is explained in text.

a small magma body show a rapid deflation curve at JRO1 followed by stabilization as the recharge rate approaches the eruption rate. Runs that involve larger magma bodies show continued long-term deflation but cannot match the rapid deflation seen in the first several weeks of the eruption. The blue solid line in figure 10*B* represents an intermediate reservoir size that shows a little deflation still after 500 days of eruption but not enough to match the data. The steep deflation at short times and the long-term continued deflation at longer times may suggest that decompression initiated within a relatively small body of eruptible magma but expanded with time to a much larger volume that may include cooler or more crystalline, partially solidified material.

Discussion and Conclusions

Within the range of uncertainty, the above results are consistent with the view that the magma reservoir at Mount St. Helens is several to perhaps a few tens of cubic kilometers in size, that the pressure drop in the magma system is several to a few tens of megapascals, and that the reservoir contains less than a few volume percent exsolved gas at the source depth of 8–9 km. Numerous uncertainties prevent us from more accurate estimates of the size, overpressure, volatile content, and degree of recharge of the Mount St. Helens magma reservoir. The greatest limitation is the uncertainty in reservoir compressibility κ_C, which appears to be at least a few times greater over the period of this eruption than during the very brief time scale of seismic wave disturbance. Our conclusion that κ_C is only a few to several times less than magma compressibility contrasts with expectations (for example, Huppert and Woods, 2002) that κ_M would be much greater than κ_C in deep, equant, volatile-saturated magma bodies. The similarity between κ_M and κ_C during this eruption likely reflects both the lower rigidity of the Earth over long time scales and the low exsolved volatile content of the magma.

The observation that geodetic deflation volume dV_C is less than erupted volume V_e is an expected consequence of the finite compressibility of magma, and need not imply recharge. We expect dV_C to be less than V_e during nearly all eruptions. Conversely, in a reservoir that is intruded before an eruption, the injection volume V_i should be significantly greater than the resulting change in reservoir volume dV_C. Deep, stiff reservoirs containing volatile-rich magmas are likely to show the lowest ratios of dV_C/V_i, raising the question of whether preeruptive magma injection into a volatile-rich reservoir might fail to generate a detectable geodetic signal.

Finally, like Huppert and Woods (2002) and Woods and Huppert (2003), we find that the compressibility of magma, which is related to exsolved volatile content, has an overriding influence on the duration and final volume of effusive eruptions. Our study, however, advances those works by showing that, when exsolution of both H_2O and CO_2 is considered, there is little or no discontinuity in compressibility at the saturation pressure, and hence no dramatic change in eruptive style or the rate of decrease in eruptive activity when the saturation pressure is reached in a magma reservoir.

The idealizations in this paper are necessary for developing a simple model. In testing our assumptions, we acknowledge that many such idealizations are unrealistic. Our simple balloon-and-soda-straw cartoon of a magma reservoir may not even approximately resemble the complex of partially molten bodies that could make up the real magma system. Given this complexity, the question of whether the magma body is being recharged may be primarily a question of where one draws boundaries. We nevertheless hope that these simple models offer some insight.

Acknowledgments

Discussion of the form of the growth curve and its relation to physical processes was initiated by Terry Gerlach and Dan Dzurisin, to whom we owe many thanks. Mike Lisowski played a crucial role gathering deformation data used in this study and was offered coauthorship but politely declined. Dan Dzurisin and Peter Cervelli reviewed this manuscript and offered several improvements. Insights into various aspects of this study were provided by John Pallister, Carl Thornber, Richard Iverson, Shaul Hurwitz, Emily Brodsky, and Seth Moran.

References Cited

Barker, S.E., and Malone, S.D., 1991, Magmatic system geometry at Mount St. Helens modeled from the stress field associated with posteruptive earthquakes: Journal of Geophysical Research, v. 96, no. B7, p. 11883–11894, doi:10.1029/91JB00430.

Blackwell, D.D., Steele, J.L., Kelley, S.A., and Korosec, M.A., 1990, Heat flow in the State of Washington and thermal conditions in the Cascade Range: Journal of Geophysical Research, v. 95, no. B12, p. 19495–19516.

Blanpied, M.L., Marone, C.J., Lockner, D.A., Byerlee, J.D., and King, D.P., 1998, Quantitative measure of the variation in fault rheology due to fluid-rock interactions: Journal of Geophysical Research, v. 103, no. B5, p. 9691–9712.

Blundy, J., and Cashman, K., 2001, Ascent-driven crystallisation of dacite magmas at Mount St. Helens, 1980–1986: Contributions to Mineralogy and Petrology, v. 140, no. 6, p. 631–650, doi:10.1007/s004100000219.

Bonaccorso, A., and Davis, P.M., 1999, Models of ground deformation from vertical volcanic conduits with application to eruptions of Mount St. Helens and Mount Etna: Journal of Geophysical Research, v. 104, no. B5, p. 10531–10542.

Brace, W.F., and Kohlstedt, D.L., 1980, Limits on lithospheric stress imposed by laboratory experiments: Journal of Geophysical Research, v. 85, no. B11, p. 6248–6252.

Byerlee, J.D., 1978, Friction of rocks: Pure and Applied Geophysics, v. 116, p. 615–626.

Byerlee, J.D., and Summers, R., 1976, A note on the effect of fault gouge thickness on fault stability [abs.]: International Journal of Rock Mechanics and Mining Sciences and Geomechanics Abstracts, v. 13, p. 35–36.

Cashman, K.V., and Taggart, J.E., 1983, Petrologic monitoring of 1981 and 1982 eruptive products from Mount St. Helens: Science, v. 221, no. 4618, p. 1385–1387.

Cashman, K.V., Thornber, C.R., and Pallister, J.S., 2008, From dome to dust; shallow crystallization and fragmentation of conduit magma during the 2004–2006 dome extrusion of Mount St. Helens, Washington, chap. 19 *of* Sherrod, D.R., Scott, W.E., and Stauffer, P.H., eds., A volcano rekindled; the renewed eruption of Mount St. Helens, 2004–2006: U.S. Geological Survey Professional Paper 1750 (this volume).

Chester, F.M., 1994, Effects of temperature on friction; constitutive equations and experiments with quartz gouge: Journal of Geophysical Research, v. 99, no. B4, p. 7247–7261.

Clauser, C., and Huenges, E., 1995, Thermal conductivity of rocks and minerals, rock physics and phase relations, *in* A handbook of physical constants: Washington D.C., American Geophysical Union, p. 105–126.

Dieterich, J.H., 1979, Modeling of rock friction 1. Experimental results and constitutive equations: Journal of Geophysical Research, v. 84, no. B5, p. 2161–2168.

Dieterich, J.H., and Kilgore, B.D., 1996, Imaging surface contacts; power law contact distributions and contact stresses in quartz, calcite, glass and acrylic plastic: Tectonophysics, v. 256, p. 216–239.

Dzurisin, D., Lisowski, M., Poland, M.P., Sherrod, D.R., and LaHusen, R.G., 2008, Constraints and conundrums resulting from ground-deformation measurements made during the 2004–2005 dome-building eruption of Mount St. Helens, Washington, chap. 14 *of* Sherrod, D.R., Scott, W.E., and Stauffer, P.H., eds., A volcano rekindled; the renewed eruption of Mount St. Helens, 2004–2006: U.S. Geological Survey Professional Paper 1750 (this volume).

Elkins, L.T., and Grove, T.L., 1990, Ternary feldspar experiments and thermodynamic models: American Mineralogist, v. 75, p. 544–559.

Fournier, R.O., 1999, Hydrothermal processes related to movement of fluid from plastic into brittle rock in the magmatic-epithermal environment: Economic Geology, v. 94, no. 8, p. 1193–1211.

Gerlach, T.M., McGee, K.A., and Doukas, M.P., 2008, Emission rates of CO_2, SO_2, and H_2S, scrubbing, and preeruption excess volatiles at Mount St. Helens, 2004–2005, chap. 26 *of* Sherrod, D.R., Scott, W.E., and Stauffer, P.H., eds., A volcano rekindled; the renewed eruption of Mount St. Helens, 2004–2006: U.S. Geological Survey Professional Paper 1750 (this volume).

Ghiorso, M.S., and Sack, R.O., 1995, Chemical mass transfer in magmatic processes IV. A revised and internally consistent thermodynamic model for the interpolation and extrapolation of liquid-solid equilibria in magmatic systems at elevated temperatures and pressures: Contributions to Mineralogy and Petrology, v. 119, p. 197–212.

Heliker, C., 1995, Inclusions in the Mount St. Helens dacite erupted from 1980 through 1983: Journal of Volcanology and Geothermal Research, v. 66, nos. 1–3, p. 115–135, doi:10.1016/0377-0273(94)00074-Q.

Huppert, H.E., and Woods, A.W., 2002, The role of volatiles in magma chamber dynamics: Nature, v. 420, no. 6915, p. 493–495.

Iverson, R.M., Dzurisin, D., Gardner, C.A., Gerlach, T.M., LaHusen, R.G., Lisowski, M., Major, J.J., Malone, S.D., Messerich, J.A., Moran, S.C., Pallister, J.S., Qamar, A.I., Schilling, S.P., and Vallance, J.W., 2006, Dynamics of seismogenic volcanic extrusion at Mount St. Helens in 2004–05: Nature, v. 444, no. 7118, p. 439–443, doi:10.1038/nature05322.

Jaeger, J.C., and Cook, N.G.W., 1979, Fundamentals of rock mechanics (3d ed.): London, Chapman and Hall, 593 p.

Johnson, D.J., Sigmundsson, F., and Delaney, P.T., 2000, Comment on "Volume of magma accumulation or withdrawal estimated from surface uplift or subsidence, with application to the 1960 collapse of Kilauea volcano" by P.T. Delaney and D.F McTigue: Bulletin of Volcanology, v. 61, p. 491–493.

Linker, M.F., and Dieterich, J.H., 1992, Effects of variable normal stress on rock friction; observations and constitutive equations: Journal of Geophysical Research, v. 97, p. 4923–4940.

Lisowski, M., Dzurisin, D., Denlinger, R.P., and Iwatsubo, E.Y., 2008, Analysis of GPS-measured deformation associated with the 2004–2006 dome-building eruption of Mount St. Helens, Washington, chap. 15 *of* Sherrod, D.R., Scott, W.E., and Stauffer, P.H., eds., A volcano rekindled; the renewed eruption of Mount St. Helens, 2004–2006: U.S. Geological Survey Professional Paper 1750 (this volume).

Marone, C., and Scholz, C.H., 1988, The depth of seismic faulting and the upper transition from stable to unstable slip regimes: Geophysical Research Letters, v. 15, no. 6, p. 621–624.

Marone, C., Raleigh, C.B., and Scholz, C.H., 1990, Frictional behavior and constitutive modeling of simulated fault gouge: Journal of Geophysical Research, v. 95, no. B5, p. 7007–7025.

Marone, C.J., Scholz, C.H., and Bilham, R., 1991, On the mechanics of earthquake afterslip: Journal of Geophysical Research, v. 96, p. 8441–8452.

Mastin, L.G., 2002, Insights into volcanic conduit flow from an open-source numerical model: Geochemistry, Geophysics, Geosystems, v. 3, no. 7, 18p., doi:10.1029/2001GC000192.

McTigue, D.F., 1987, Elastic stress and deformation near a finite spherical magma body; resolution of the point source paradox: Journal of Geophysical Research, v. 92, no. B12, p. 12931–12940.

Mironer, A., 1979, Engineering fluid mechanics: New York, McGraw-Hill, 592 p.

Moore, P.L., Iverson, N.R., and Iverson, R.M., 2008, Frictional properties of the Mount St. Helens gouge, chap. 20 *of* Sherrod, D.R., Scott, W.E., and Stauffer, P.H., eds., A volcano rekindled; the renewed eruption of Mount St. Helens, 2004–2006: U.S. Geological Survey Professional Paper 1750 (this volume).

Musumeci, C., Gresta, S., and Malone, S.D., 2002, Magma system recharge of Mount St. Helens from precise relative hypocenter location of microearthquakes: Journal of Geophysical Research, v. 107, no. B10, 2264, p. ESE 16-1–ESE 16-9, doi:10.1029/2001JB000629.

Newhall, C.G., and Melson, W.G., 1983, Explosive activity associated with the growth of volcanic domes: Journal of Volcanology and Geothermal Research, v. 17, p. 111–131.

Newman, A.V., Dixon, T.H., Ofoegbu, G.I., and Dixon, J.E., 2001, Geodetic and seismic constraints on recent activity at Long Valley Caldera, California; evidence for viscoelastic rheology: Journal of Volcanology and Geothermal Research, v. 105, no. 3, p. 183–206.

Newman, A.V., Dixon, T.H., and Gourmelen, N., 2006, A four-dimensional viscoelastic deformation model for Long Valley Caldera, California, between 1995 and 2000: Journal of Volcanology and Geothermal Research, v. 150, nos. 1–3, p. doi:10.1016/j.jvolgeores.2005.1007.1017.

Newman, S., and Lowenstern, J.B., 2002, VolatileCalc; a silicate melt-H_2O-CO_2 solution model written in Visual Basic for Excel®: Computers and Geosciences, v. 28, no. 5, p. 597–604, doi:10.1016/S0098-3004(01)00081-4.

Pallister, J.S., Thornber, C.R., Cashman, K.V., Clynne, M.A., Lowers, H.A., Mandeville, C.W., Brownfield, I.K., and Meeker, G.P., 2008, Petrology of the 2004–2006 Mount St. Helens lava dome—implications for magmatic plumbing and eruption triggering, chap. 30 *of* Sherrod, D.R., Scott, W.E., and Stauffer, P.H., eds., A volcano rekindled; the renewed eruption of Mount St. Helens, 2004–2006: U.S. Geological Survey Professional Paper 1750 (this volume).

Poland, M.P., and Lu, Z., 2008, Radar interferometry observations of surface displacements during pre- and coeruptive periods at Mount St. Helens, Washington, 1992–2005: chap. 18 *of* Sherrod, D.R., Scott, W.E., and Stauffer, P.H., eds., A volcano rekindled; the renewed eruption of Mount St. Helens, 2004–2006: U.S. Geological Survey Professional Paper 1750 (this volume).

Pollard, D.D., and Fletcher, D.F., 2005, Fundamentals of structural geology: Cambridge, Cambridge University Press, 500 p.

Power, W.L., Tullis, T.E., and Weeks, J.D., 1988, Roughness and wear during brittle faulting: Journal of Geophysical Research, v. 93, no. B12, p. 15268–15278.

Reinen, L.A., Weeks, J.D., and Tullis, T.E., 1994, The frictional behavior of lizardite and antigorite serpentinites; experiments, constitutive models, and implications for natural faults: Pure and Applied Geophysics, v. 143, p. 317–358.

Robertson, E.C., 1983, Relationship of fault displacement to gouge and breccia thickness: Mining Engineering, v. 35, p. 1426–1432.

Rubin, A.M., 1990, A comparison of rift-zone tectonics in Iceland and Hawaii: Bulletin of Volcanology, v. 52, p. 302–319.

Ruina, A., 1983, Slip instability and state variable friction laws: Journal of Geophysical Research, v. 88, no. B12, p. 10359–10370.

Rutherford, M.J., and Devine, J.D., 1988, The May 18, 1980, eruption of Mount St. Helens; 3, Stability and chemistry of amphibole in the magma chamber: Journal of Geophysical Research, v. 93, no. B10, p. 11949–11959.

Rutherford, M.J., and Devine, J.D., III, 2008, Magmatic conditions and processes in the storage zone of the 2004–2006 Mount St. Helens dacite, chap. 31 *of* Sherrod, D.R., Scott, W.E., and Stauffer, P.H., eds., A volcano rekindled; the renewed eruption of Mount St. Helens, 2004–2006: U.S. Geological Survey Professional Paper 1750 (this volume).

Rutherford, M.J., Sigurdsson, H., Carey, S., and Davis, A., 1985, The May 18, 1980, eruption of Mount St. Helens; 1, Melt composition and experimental phase equilibria: Journal of Geophysical Research, v. 90, no. B4, p. 2929–2947.

Scandone, R., and Malone, S.D., 1985, Magma supply, magma discharge and readjustment of the feeding system of Mount St. Helens during 1980: Journal of Volcanology and Geothermal Research, v. 23, nos. 3–4, p. 239–262, doi:10.1016/0377-0273(85)90036-8.

Schaff, D.P., Beroza, G., and Shaw, B.E., 1999, Postseismic response of repeating aftershocks: Geophysical Research Letters, v. 25, p. 4559–4552.

Schilling, S.P., Thompson, R.A., Messerich, J.A., and Iwatsubo, E.Y., 2008, Use of digital aerophotogrammetry to determine rates of lava dome growth, Mount St. Helens, Washington, 2004–2005, chap. 8 *of* Sherrod, D.R., Scott,

W.E., and Stauffer, P.H., eds., A volcano rekindled; the renewed eruption of Mount St. Helens, 2004–2006: U.S. Geological Survey Professional Paper 1750 (this volume).

Scholz, C.H., 1998, Earthquakes and friction laws: Nature, v. 391, p. 37–42.

Stasiuk, M.V., Jaupart, C., and Sparks, R.S.J., 1993, On the variations of flow rate in non-explosive lava eruptions: Earth and Planetary Science Letters, v. 134, p. 505–516.

Tait, S., Jaupart, C., and Vergniolle, S., 1989, Pressure, gas content and eruption periodicity of a shallow, crystallising magma chamber: Earth and Planetary Science Letters, v. 92, p. 107–123.

Tiampo, K.F., Rundle, J.B., Fernandez, J., and Langbein, J.O., 2000, Spherical and ellipsoidal volcanic sources at Long Valley caldera, California, using a genetic algorithm inversion technique: Journal of Volcanology and Geothermal Research, v. 102, p. 189–206.

Turcotte, D.L., and Schubert, G., 2002, Geodynamics (2d ed.): Cambridge, Cambridge University Press, 456 p.

Wadge, G., 1981, The variation of magma discharge during basaltic eruptions: Journal of Volcanology and Geothermal Research, v. 11, p. 139–168.

Williams, D.L., Abrams, G., Finn, C., Dzurisin, D., Johnson, D.J., and Denlinger, R., 1987, Evidence from gravity data for an intrusive complex beneath Mount St Helens: Journal of Geophysical Research, v. 92, no. B10, p. 10207–10222.

Woods, A.W., and Huppert, H.E., 2003, On magma chamber evolution during slow effusive eruptions: Journal of Geophysical Research, v. 108, no. B8, 2403, p. doi:10.1029/2002JB002019.

Zoback, M.D., and Healy, J.H., 1984, Friction, faulting, and in situ stress: Annalen der Geophysik, v. 2, p. 689–698.

Appendix 1. Processes That Could Affect Reservoir Compressibility

The static shear modulus of large rock masses (kilometers in size) is generally known to be up to an order of magnitude less than that of laboratory-scale specimens (Pollard and Fletcher, 2005, p. 322). The reduction in shear modulus with increasing scale is generally attributed to the presence of fractures that can open or move (Rubin, 1990). In this paper we estimate host-rock shear modulus from the velocities of seismic waves whose wavelength is on the order of a kilometer and does not differ greatly from the dimensions of the rock mass under stress near the magma reservoir. On the other hand, seismic velocities are controlled by stress oscillations that act over a time scale of milliseconds, whereas eruption-associated stress changes evolve over a period of years. Over the longer time scale, subcritical crack growth, poroelasticity, and inelastic creep could deform rock and therefore reduce the shear modulus, G. Because the geodetic signal is measured at the surface, a low shear modulus at shallow depth could perhaps also affect the geodetic signal. These effects are considered below.

Crack growth and poroelasticity.—Crack growth may greatly reduce G at <1–2 km depth (Rubin, 1990), but at 6–12 km depth it is unclear whether cracks of any significant size exist. Near the hot reservoir, cracks are likely to anneal and seal off interstitial fluids (Fournier, 1999). Poroelastic effects theoretically have no effect on shear modulus, though they can decrease Poisson's ratio with time and change estimates of G if such estimates are based on the formula $G = \rho_R \upsilon_P^2 (1-2\nu)/(2(1-\nu))$ (for example, Rubin, 1990). Poroelastic effects, however, change G by only a few tens of percent at most; at depths of 6–12 km, interstitial fluids are likely sparse and these effects even smaller.

Elastic inhomogeneity.—Figure 5 shows variations in G with depth estimated from the seismic-velocity profile and density data (explained in the figure caption). In the uppermost 1–2 km the estimated value of G may drop to about 11 GPa; however, at depths below 1–2 km the value of G remains above about 35 GPa. Because the surface displacements are affected by the elastic properties of all materials between the magma reservoir and the surface, the lower elastic moduli of near-surface materials must affect displacements to some degree, but the relation between reservoir stress drop and displacement should be primarily controlled by rock properties near the magma body. For this reason we consider that the effect of less stiff near-surface materials on G is likely to be less than about 20 percent.

High-temperature inelastic deformation near the magma body.—In long-lived magma systems, such as Long Valley in eastern California, viscoelastic creep may reduce by about two-thirds the pressure change required for a given volume change (Newman and others, 2001; Newman and others, 2006). However, the Mount St. Helens magma system is relatively young and surrounded by cooler rock that is gabbroic in composition (Heliker, 1995) and resistant to creep. Regional heat-flow studies suggest that the ambient temperature at 9–10 km depth in this region is about 350°C (Blackwell and others, 1990). If we assume the magma reservoir has existed at its present temperature for about 4,000 to 40,000 years, we can estimate the temperature profile around the magma reservoir by numerically integrating the following one-dimensional transient equation for conductive heat flow:

$$\frac{\partial T}{\partial t} = \frac{k_R}{\rho_R c_R r} \frac{\partial}{\partial r}\left(r \frac{\partial T}{\partial r} \right), \tag{35}$$

where k_R and c_R are the thermal conductivity and specific heat, respectively, of the host rock, and r is the radial distance of a given point from the center of the magma body. Holding the temperature at the reservoir wall constant at 850°C and using $k_R = 2$ W/(m·K) (Clauser and Huenges, 1995) and $c_R = 1{,}300$ J/

(kg·K), we obtain the temperature profiles from a 1-km-radius magma body illustrated in figure 12*A*.

If decompression is rapid, the host rock will deform elastically, then relax with time as viscous creep reduces wall stress. The equations for the radial (σ_{rr}) and normal ($\sigma_{\theta\theta}$) stresses near a cylindrical body in an infinite linear elastic medium under plane-strain conditions are (Jaeger and Cook, 1979, p. 251):

$$\sigma_{rr} = \sigma_1\left(1-\frac{R^2}{r^2}\right)+p\left(\frac{R^2}{r^2}\right) \quad , \tag{36}$$

$$\sigma_{\theta\theta} = \sigma_1\left(1+\frac{R^2}{r^2}\right)-p\left(\frac{R^2}{r^2}\right) \quad , \tag{37}$$

where σ_1 is the far-field normal stress (assumed equal in all directions perpendicular to the cylinder axis), p is the internal pressure in the reservoir, and R is the cylinder radius. For $\sigma_1 = 240$ MPa and $p = 210$ MPa, values of σ_{rr} and $\sigma_{\theta\theta}$ are plotted in figure 12*B*. Note that at the reservoir wall, the difference $\sigma_{\theta\theta}-\sigma_{rr}$ is equal to twice (σ_1-p).

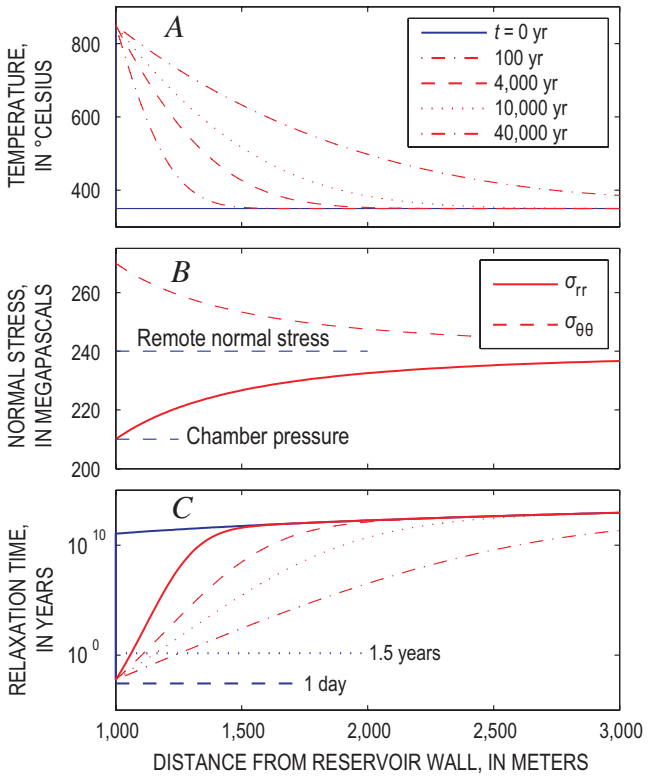

Figure 12. Response of a 1-km-radius magma body through time, as a function of distance from reservoir walls. *A*, Temperature over increasing time periods since emplacement of the magma body. Temperatures were calculated by integrating equation 35 with time. *B*, Circumferential ($\sigma_{\theta\theta}$) and radial (σ_{rr}) normal stresses versus radial distance from the reservoir wall, calculated assuming elastic deformation at short time periods following a rapid pressure change in the magma body. *C*, Viscous relaxation time versus distance for hot rock. The solid blue curve shows relaxation time versus distance assuming the host rock has a uniform temperature of 350°C. Red curves give relaxation time assuming the host-rock temperature varies with distance from the reservoir wall as illustrated by corresponding curves in panel *A*.

The dominant form of stress relaxation is likely to be dislocation creep (Turcotte and Schubert, 2002), which involves a power-law dependence between normal strain rate ($\dot{\varepsilon}_{\theta\theta}$ or $\dot{\varepsilon}_{rr}$) and normal-stress difference ($\sigma_{\theta\theta}-\sigma_{rr}$) (Turcotte and Schubert, 2002, eq. 7-187):

$$\dot{\varepsilon}_{rr} = -\dot{\varepsilon}_{\theta\theta} = C_1\left(\sigma_{\theta\theta}-\sigma_{rr}\right)^n e^{-E_a/R_gT}, \tag{38}$$

where C_1, n, and E_a are fitting parameters, R_g is the gas constant, and T is temperature (in Kelvin). We use $C_1 = 520$ MPa^{-n}/s, $n = 3$, and $E_a = 356$ kJ/mol, which are appropriate for diabase (Turcotte and Schubert, 2002, table 7-4). The power-law dependence implies that viscosity is not constant at a given temperature; however, we can estimate a rough average viscosity from the relation:

$$\eta_{eff} \approx \frac{\left(\sigma_{\theta\theta}-\sigma_{rr}\right)}{\dot{\varepsilon}_{rr}} = \frac{e^{-E_a/RT}}{C_1\left(\sigma_{\theta\theta}-\sigma_{rr}\right)^{n-1}}. \tag{39}$$

Using this viscosity and Young's modulus $E = \rho v_P^2(1-2\nu)(1+\nu)/(1-\nu) = 1\times10^{11}$ Pa, (where $\nu = 0.25$, $v_P = 6.6$ km/s and $\rho = 2{,}700$ kg/m^3), the viscous relaxation time τ_η is:

$$\tau_\eta = \frac{\eta_{eff}}{E}. \tag{40}$$

Rocks having $\eta_{eff} < \sim 5\times10^{18}$ Pa·s will relax in less time than the 1.5-year duration of the eruption to date (early 2006). For a magma body that has existed for about 4,000–40,000 years, rocks within ~110–250 m of the reservoir wall will relax within this time period. If these rocks are considered part of the mechanical magma reservoir, its effective volume would be about 20 percent to 50 percent greater than the volume of magma alone. By comparison, no host rock was hot enough to relax during the 24-hour period following the Mount St. Helens eruptions of May and June 1980 (fig. 12*C*). Thus the aseismic body identified by Scandone and Malone (1985) could be as much as a few hundred meters smaller in diameter than the mechanical magma body that is deforming during the current eruption.

Appendix 2. Derivation of the Exponential Equation

Derivation of the exponential relation involves differentiating equation 11:

$$\frac{dp}{dt} = -C\left(\frac{dM_e}{dt}-Q_i\right) \tag{41}$$

and substituting equation 12 into this equation to give:

$$\frac{dp}{dt} = BC + CQ_i - ACp \,. \tag{42}$$

Reversing the denominator in the left-hand term with the right-hand side of the equation and integrating gives:

$$-\frac{1}{AC}\ln\left(BC + CQ_i - ACp\right) + C_2 = t \,, \tag{43}$$

where C_2 is the constant of integration. We find a value for C_2 by noting that, at $t=0$, $p=p_0$; hence

$$-\frac{1}{AC}\ln\left[\frac{BC + CQ_i - ACp}{BC + CQ_i - ACp_0}\right] =$$

$$-\frac{1}{AC}\ln\left[1 + \frac{AC\left(p_0 - p\right)}{BC + CQ_1 - ACp_0}\right] = t \,. \tag{44}$$

Further rearrangement leads to:

$$p = p_0 - \left(p_0 - \frac{B + Q_i}{A}\right)\left(1 - e^{-ACt}\right) \,. \tag{45}$$

This equation can be substituted into equation 12 to give:

$$\frac{dM_e}{dt} = Ap_0 + \left(B + Q_i - Ap_0\right)\left(1 - e^{-ACt}\right) - B$$
$$= Q_i - \left(B + Q_i - Ap_0\right)e^{-ACt} \,, \tag{46}$$

which can be integrated to give:

$$M_e = Qt + \frac{B + Q_i - Ap_0}{AC}e^{-ACt} + C_2 \,, \tag{47}$$

where C_2 is a constant of integration, which can be evaluated by noting that, at $t=0$, $M_e=0$. After evaluating C_2, we get:

$$M_e = \frac{\left(Ap_0 - B\right) - Q_i}{AC}\left(1 - e^{-ACt}\right) + Q_i t \,. \tag{48}$$

This equation can be expressed in eruptive volume (V_e) by dividing by lava density ρ_e:

$$V_e = \frac{1}{\rho_e}\frac{\left(Ap_0 - B\right) - Q_i}{AC}\left(1 - e^{-ACt}\right) + \frac{Q_i}{\rho_e}t \,. \tag{49}$$

Appendix 3. The Exponential Equation for "Greased Plug" Flow

The assumption of Newtonian flow implies that the flow profile in the conduit is parabolic. Given the high crystal content of the magma, a more realistic scenario may be that the magma in the center of the conduit moves upward as a solid plug and that shear is concentrated along the conduit margins (fig. 8*B*). If the material in the shear acts in a Newtonian manner, a force balance leads to the following equation:

$$\pi R^2 p - \rho\, g\pi R^2 H - \frac{2H\eta}{\rho R\Delta r}\frac{dM_e}{dt} = 0 \,, \tag{50}$$

where Δr is the thickness of the shear zone and ρ is the magma density in the conduit. The first term is the upward force at the base of the conduit, the second is the weight of the magma plug, and the third is the viscous force resisting upward flow. The equation can be rearranged as:

$$\frac{dM_e}{dt} = \frac{\rho\pi R^3\Delta r}{2\eta H}\left(p - \rho gH\right) \,. \tag{51}$$

In this case, the terms A and B in equation 12 have the value $A=\rho\pi R^3\Delta r/(8\eta H)$ and $B=\pi R^3\Delta r\rho^2 g/(8\eta)$. Substitution of these terms into equations 14 and 15 leads to expressions for a and b that are identical to equations 18 and 20; hence the constraints on the product $V_C(p_0-\rho_m gH)$ are exactly the same for greased-plug flow as for Newtonian flow.

Appendix 4. Exponential Equation for Newtonian Flow Capped by a Frictional Plug with Constant Frictional Properties

The presence of fault gouge along the dome surface at Mount St. Helens suggests that, over some distance near the surface, magma moves upward as a solid plug with frictional sliding along its margins (fig. 8*D*). Assuming that flow below this plug is Newtonian, the equation for mass flux is:

$$\frac{dM_e}{dt} = \frac{\rho\pi R^4}{8\eta H_1}\left(\left(p - p_1\right) - \rho gH_1\right) \,, \tag{52}$$

where H_1 is the length of conduit over which flow is Newtonian and p_1 is the pressure at the base of the frictional plug (fig. 8*C*). That pressure is a function of both plug weight and friction. We assume that the shear stress along the plug margin must exceed the normal stress (σ_n) times a coefficient of friction (μ), which is assumed to be constant:

$$\tau \geq \mu\sigma_n \,. \tag{53}$$

If the plug is cylindrical, vertical, of the same radius (R) as the conduit below, and of length H_2, the pressure (p_1) at the base of an upward-moving plug must exceed the sum of the plug weight and the frictional resistance:

$$p_1 \geq \rho gH_2 + \frac{2\,\mu\overline{\sigma}_n H_2}{R} \,. \tag{54}$$

In this case, $\overline{\sigma}_n$ represents the mean normal stress on the conduit walls over the length of the plug. In solid rock, the horizontal normal stress could vary greatly even at shallow depth, depending on the state of gas pressure and on geometric factors. On the other hand, at Mount St. Helens, the crater floor is composed primarily of unconsolidated fallback from the 1980

eruptions. If we take this material to be cohesionless, faults of favorable orientation will form when the ratio of effective normal to shear stress on any potential fault plane exceeds that allowed by the coefficient of friction of the material (μ_h). Thus the ratio of most compressive (σ_1) to least compressive (σ_3) normal principal stress at any depth is limited to (Brace and Kohlstedt, 1980; Zoback and Healy, 1984):

$$\frac{\sigma_1 - p_p}{\sigma_3 - p_p} \le \left[\mu_h + \left(\mu_h^2 + 1\right)^{1/2} \right]^2 , \qquad (55)$$

where p_p is the pore pressure in the host rock. For $\mu_h = 0.6$ and p_p ranging from 0 to σ_3, σ_1/σ_3 ranges from 1 to ~3. For this reason, we consider the normal stress on the conduit wall to be one-third to three times the vertical stress, and express the normal stress as the vertical stress times a constant γ of order 1. If the frictional plug extends from the surface to a depth H_2, the mean normal stress on the plug wall is $\bar{\sigma}_n = \gamma \bar{\rho} g H_2 / 2$. We also assume that $\mu \cong 0.5$; these simplifications allow us to rewrite equation 54 as:

$$p_1 \approx \rho g H_2 \left(1 + \gamma \frac{H_2}{R}\right). \qquad (56)$$

Inserting this value into equation 52 and noting that $H_1 + H_2 = H$, we have:

$$\frac{dV_e}{dt} = \frac{1}{\rho_e} \frac{\rho \pi R^4}{8 \eta H_1} \left(p - \bar{\rho} g \left(H + \gamma \frac{H_2}{R} \right) \right). \qquad (57)$$

Hence $A = \rho_e \pi R^4/(8\eta H_1)$ and $B = \pi R^4 \rho_e^2 g(H + \gamma H_2/R)/(8\eta H_1)$. These terms lead to the following values of a and b:

$$a = \frac{\left(dV_e/dt\right)_{t=0} - \left(dV_e/dt\right)_{t\to\infty}}{\frac{\rho_M}{\rho_e}\left(\frac{dV_e}{dt}\right)_{t=0} \frac{K_M}{V_C\left(p_0 - \bar{\rho} g \left(H + \gamma \frac{H_2}{R}\right)\right)}}$$

$$\approx 0.8 \frac{V_C\left(p_0 - \bar{\rho} g \left(H + \gamma \frac{H_2}{R}\right)\right)}{K_M} , \qquad (58)$$

$$b = AC = \frac{\rho_e}{\rho_M}\left(\frac{dV_e}{dt}\right)_{t=0} \frac{K_M}{V_C\left(p_0 - \bar{\rho} g \left(H + \gamma \frac{H_2}{R}\right)\right)}. \qquad (59)$$

Appendix 5. Exponential Equation for "Greased Plug" Flow Capped by a Frictional Plug with Constant Frictional Properties

As with the case above (appendix 4), this case involves modifying the greased plug equation to include a term for the pressure at the base of the frictional plug:

$$\frac{dM_e}{dt} = \frac{\rho \pi R^3 \Delta r}{2 \eta H_1} \left((p - p_1) - \rho g H_1 \right). \qquad (60)$$

Inserting the expression for p_1 in equation 56, we have:

$$\frac{dM_e}{dt} = \frac{\rho \pi R^3 \Delta r}{2 \eta H_1} \left[p - \rho g \left(H + \gamma \frac{H_2}{R} \right) \right]. \qquad (61)$$

Hence $A = \rho \pi R^3 \Delta r/(2\eta H_1)$ and $B = \pi R^3 \Delta r \rho^2 g(H + \gamma H_2/R)/(2\eta H_1)$.

Appendix 6. Derivation of Logarithmic Growth Curve

We envision a one-dimensional system consisting of a magma-filled reservoir and conduit system applying a pressure p to the base of an extruding solid rock plug of mass M_p and displacement rate $\dot{\delta}$ against gravity and frictional resistance to slip between the plug and the conduit wall. The rate of extrusion is controlled entirely by frictional resistance. That is, in this end-member model the magma below the plug has negligible viscosity.

Plug force balance.—Consider a "quasi-static" force balance for motion of a cylindrical plug (force resulting from acceleration is assumed to be negligible, $M\, d\dot{\delta}/dt \approx 0$). This quasi-static assumption is well justified by results of simulations in which inertia is considered; these "dynamic" simulations are not discussed in this appendix or elsewhere in this paper. The plug mass is assumed to be constant ($dM_p/dt \approx 0$), resulting from a balance between the rate of surface erosion of the plug and an equivalent subsurface accretion rate (for example, Iverson and others, 2006). The force balance per unit cross-sectional area in the conduit is:

$$p = \frac{M_p g}{\pi R^2} + \frac{2\tau H_2}{R} , \qquad (62)$$

where p is the fluid pressure of the magma applied to the base of the plug, R is plug radius, H_2 is plug height, g is the acceleration due to gravity, and τ is the shear resistance of the interface between the plug and the conduit wall. Because the mass is assumed constant, R and H_2 are also constant.

Faults have a well-known second-order dependence of shear strength on slip rate $\dot{\delta}$ (Dieterich, 1979; Ruina, 1983) and related, somewhat complicated dependencies on accumulated slip and time of contact ("state" effects in rate and state friction) (for example, Linker and Dieterich, 1992). However, fault strength can be assumed to be purely slip-rate dependent when subject to sustained sliding if the ratio of asperity contact size to slip rate is small relative to the duration of sustained slip. Daily extrusion rates at Mount St. Helens from October 2004 to October 2005, converted to boundary slip rates, are in the range 70 to 7,000 μm/s, assuming that the plug has radius in the range of 25 to 75 m. Taking asperity contact size to be no more than 20 μm, as laboratory data on rock

friction suggest (for example, Dieterich and Kilgore, 1996), its ratio to slip rate is 0.29 to 0.0029 seconds, meaning that time-dependent and slip-dependent changes and friction can be ignored for sustained slip durations longer than 0.5 to 1.0 seconds. Data on extruded volume are collected over intervals of a few weeks to a month. Therefore, we ignore complicated "state" effects on fault shear strength, and represent it by a simple slip-rate-dependent relation,

$$\tau = \tau_o + A_1\sigma_n \ln\frac{\dot{\delta}}{\dot{\delta}_o} \ . \tag{63}$$

Here σ_n is normal stress at the wall and A_1 is the rate dependence of fault strength. The constant τ_o is an arbitrary reference, the strength of the wall interface when the interface slip rate is $\dot{\delta}_o$.

For shear of thick fault-gouge layers (for example, Byerlee and Summers, 1976; Marone and others, 1990), for shear near the brittle-ductile transition (for example, Blanpied and others, 1998), and for near-surface faulting (Marone and Scholz, 1988), fault strength increases with slip rate (velocity strengthening, rate strengthening). Because all of these conditions are present at the plug wall at Mount St. Helens, we expect that fault slip is predominantly rate strengthening, and thus A_1 in equation 63 is a small positive constant, typically between 0.001 and 0.03 (Marone and Scholz, 1988; Blanpied and others, 1998).

The volume of extruded material V_e is the product of the conduit cross-sectional area and the slip at the wall, and the extruded mass M_e is proportional to the extruded volume, so equation 63 is equivalently

$$\tau = \tau_o + A_1\sigma_n \ln\frac{\dot{M}_e}{\dot{M}_o} \ , \tag{64}$$

where notation for the mass rate of extrusion $dM_e/dt = \dot{M}_e$ is used. Combining equations 62 and 64 leads to a relation between magma pressure and the rate of plug extrusion

$$p = p_o + a\ln\frac{\dot{M}_e}{\dot{M}_o} \ , \tag{65}$$

where $a = 2A_1\sigma_n H_2/R$ and $p_0 = 2\tau_0 H_2/R + Mg/\pi R^2$ are constants.

Magma mass balance.—During plug extrusion, the volume and driving pressure of the magma will change. To characterize these changes we consider, in turn, mass and volume balances for the magma. We define the magma mass $M_M = \rho_M V_M$ as the mass of magma in the magma reservoir and in the conduit below the frictional plug. The rate of change of mass can be expressed as

$$\frac{dM_M}{dt} = \rho_M \frac{dV_M}{dt} + V_M \frac{d\rho_M}{dt} \ , \tag{66}$$

where ρ_M and V_M are magma density and volume, respectively. The mass change rate is also equivalent to the difference between the rate of mass input to the system Q_i and the rate out of the system Q_o, or

$$\frac{dM_M}{dt} = Q_i - Q_o \ . \tag{67}$$

Because magma is not being extruded at the surface, Q_o represents the magma-volume loss due to magma freezing onto the plug (Iverson and others, 2006). Combining and rearranging so that fluid volume is the dependent variable yields

$$\frac{dV_M}{dt} = -\frac{V_M}{\rho_M}\frac{d\rho_M}{dt} + \frac{Q_i}{\rho_M} - \frac{Q_o}{\rho_M} \ . \tag{68}$$

Reference to the magma density and its time derivative can be replaced by the pressure dependence through expanding the density derivative in equation 68:

$$\frac{d\rho_M}{dt} = \frac{\partial\rho_M}{\partial p}\frac{dp}{dt} \tag{69}$$

and using the definition of the elastic compressibility of the magma $\kappa_M \equiv (1/\rho_M)(\partial\rho_M/\partial p)$. Making these substitutions into equation 68 leads to

$$\frac{dp}{dt} = -\frac{1}{V_M\kappa_M}\left(\frac{dV_M}{dt} + \frac{Q_o}{\rho_M} - \frac{Q_i}{\rho_M}\right). \tag{70}$$

Magma volume balance.—The volume of the magma system increases as the solid plug is extruded at a rate dV_e/dt, and decreases as magma freezes to the plug at the rate $-Q_o/\rho_M$. We also allow the walls of the magma system (reservoir and conduit) to respond elastically to changes in magma pressure using a representative reservoir and conduit compressibility κ_c so that the rate of elastic change of magma volume is $\kappa_c V_M\, dp/dt$. The combined rate of magma volume change is then

$$\frac{dV_M}{dt} = \frac{dV_e}{dt} - \frac{Q_o}{\rho_M} + \kappa_c V_M \frac{dp}{dt} \ . \tag{71}$$

Combining equations 70 and 71 yields the relation between the mass rate of extrusion and the rate of change of the driving pressure

$$\frac{dp}{dt} = -\frac{\dot{M}_e/\rho_e - Q_i/\rho_M}{V_M(\kappa_C + \kappa_M)} \ , \tag{72}$$

where the extruded mass is $M_e = V_e\rho_e$.

Solutions

Solutions for extrusion rate with time can be found by taking the time derivative of equation 65

$$\frac{dp}{dt} = \frac{a}{\dot{M}_e}\frac{d\dot{M}_e}{dt} \tag{73}$$

and equating to equation 71, resulting in the single differential equation

$$\frac{d\dot{M}_e}{dt} = -\frac{1}{aV_M(\kappa_c + \kappa_M)}\left(\frac{\dot{M}_e{}^2}{\rho_e} - \frac{\dot{M}_e Q_i}{\rho_M}\right). \tag{74}$$

If the magma volume is large relative to the extruded volume, then V_M can be treated as a constant and equation 74 is separable. In the solution that follows we assume negligible density contrast between the magma and plug, $\rho_e = \rho_M$, as justified elsewhere in this paper.

No Recharge.—When $Q_i = 0$ the extrusion rate is:

$$\dot{M}_e = \frac{D a \dot{M}_0}{t\dot{M}_0 / \rho_e + aD}, \tag{75}$$

where $\dot{M}_0$ is the extrusion rate at $t = 0$, and $D = V_M(\kappa_C + \kappa_M)$. The cumulative mass of extruded material goes as

$$M_e = \rho_e a D \ln\left(1 + \frac{t\dot{M}_0}{\rho_e D a}\right). \tag{76}$$

This is the logarithmic form that well characterizes stress relaxation due to fault slip in some laboratory experiments (Reinen and others, 1994) and during earthquake afterslip (for example, Marone and others, 1991; Schaff and others, 1999).

With recharge.—If $Q_i > 0$ the extrusion rate is

$$\dot{M}_e = \frac{Q_i}{1 - \left(1 - \frac{Q_i}{\dot{M}_0}\right) e^{\frac{-Q_i t}{\rho_e a D}}}. \tag{77}$$

Note that equation 77 is for $Q_i > 0$ and does not easily reduce to equation 75 for $Q_i = 0$.

Cumulative extruded mass goes as

$$M_e = \rho_e a D \ln\left[1 - \frac{\dot{M}_0}{Q_i}\left(1 - e^{\frac{Q_i t}{\rho_e a D}}\right)\right]. \tag{78}$$

This expression can be converted to erupted volume V_e by dividing by ρ_e.